Chemical Engineering Journal

Coal gasification process driven by concentrated solar radiation for carbon neutralization: reaction and energy characteristics

--Manuscript Draft--

Manuscript Number:	CEJ-D-22-11866R2
Article Type:	Research Paper
Keywords:	Solar energy; radiation gasification; Thermochemical conversion; catalytic; Kinetics
Corresponding Author:	Shiquan Shan, ph.D Zhejiang University CHINA
First Author:	Qi Zhang
Order of Authors:	Qi Zhang
	Shiquan Shan, ph.D
	Jinhong Yu
	Zhijun Zhou
	Kai H. Luo
Abstract:	Solar-driven gasification products for chemical feedstock are one of the effective means to utilize coal in a low-carbon and resourceful way. However, few studies on the reaction and energy characteristics are based on experimental data of concentrated solar coal gasification. This study designed a novel experimental solar radiation gasification thermogravimetric device. An energy model of a solar radiation dish thermochemical conversion system was also developed. Compared to indirect radiation, direct radiation has a 10 % higher carbon conversion rate, an increased energy upgrade factor (up to 0.86), and a 38.5 % increase in energy conversion efficiency. Furthermore, we investigate direct radiation-catalyzed gasification to assess the effects of different types and ratios of catalysts. The results showed that the catalytic effect of K2CO3 was better than that of Na2CO3, which would improve the energy conversion efficiency by 4.8 %. For K2CO3, the efficiency was increased by 14.1 % through increasing the doping ratio from 5 % to 10 %. Meanwhile, this study analyzed the reaction kinetics of direct radiation-catalyzed gasification. Finally, we constructed a solar concentrating radiation dish thermochemical conversion system model based on the experimental data. We found that the system energy efficiency in the direct radiation form was 15.3 % higher than that in the indirect radiation form; besides, adding the catalyst in the direct radiation form increased the energy efficiency by 23.8%. We also found that the gasifier exergy efficiency in direct radiation catalyst gasification was 29.7%, and that of indirect radiation gasification was 7.23 %. The monthly solar exergy distribution follows the solar radiation closely. The results guide the chemical process of solar thermal conversion.
Response to Reviewers:	

Coal gasification process driven by concentrated solar radiation for carbon neutralization: reaction and energy characteristics

Qi Zhang[a,b], Shiquan Shan [a, *], Jinhong Yu [a], Zhijun Zhou [a], Kai H. Luo [b]

[a] *State Key Laboratory of Clean Energy Utilization, Zhejiang University, Hangzhou 310027, Zhejiang, P.R. China;* [b.] *Department of Mechanical Engineering, University College London, Torrington Place, London WC1E 7JE, UK*

*Corresponding author e-mail: shiquan1204@zju.edu.cn

Abstract

Solar-driven gasification products for chemical feedstock are one of the effective means to utilize coal in a low-carbon and resourceful way. However, few studies on the reaction and energy characteristics are based on experimental data of concentrated solar coal gasification. This study designed a novel experimental solar radiation gasification thermogravimetric device. An energy model of a solar radiation dish thermochemical conversion system was also developed. Compared to indirect radiation, direct radiation has a 10 % higher carbon conversion rate, an increased energy upgrade factor (up to 0.86), and a 38.5 % increase in energy conversion efficiency. Furthermore, we investigate direct radiation-catalyzed gasification to assess the effects of different types and ratios of catalysts. The results showed that the catalytic effect of K_2CO_3 was better than that of Na_2CO_3, which would improve the energy conversion efficiency by 4.8 %. For K_2CO_3, the efficiency was increased by 14.1 % through increasing the doping ratio from 5 % to 10 %. Meanwhile, this study analyzed the reaction kinetics of direct radiation-catalyzed gasification. Finally, we constructed a solar concentrating radiation dish thermochemical conversion system model based on the experimental data. We

found that the system energy efficiency in the direct radiation form was 15.3 % higher than that in the indirect radiation form; besides, adding the catalyst in the direct radiation form increased the energy efficiency by 23.8 %. We also found that the gasifier exergy efficiency in direct radiation catalyst gasification was 29.7 %, and that of indirect radiation gasification was 7.23 %. The monthly solar exergy distribution follows the solar radiation closely. The results guide the chemical process of solar thermal conversion.

Keywords: solar energy; radiation gasification; thermochemical conversion; catalytic; kinetics

1 Introduction

Coal has massive reserves, and its use as a fuel for a long time has resulted in significant carbon emissions. In recent years, many countries have announced carbon-neutral energy policies. It is necessary to capture carbon in the energy production process [1] and develop renewable energy [2]. Therefore, the proportion of coal used as a fuel is gradually decreasing. But low-carbon emission utilization of coal is an essential research theme in the face of its huge reserves. Coal gasification is a vital means of clean and efficient utilization [3]. It can generate syngas and is a main feedstock for the chemical industry. The traditional process uses the heat from combustion to power the gasification, which does not meet carbon-neutral requirements. Therefore, renewable energy sources such as solar energy are required to drive the coal gasification process.

Solar energy is the primary sustainable energy source. The solar-driven coal gasification is based on a solar thermochemical energy conversion process. Researchers initiated thermochemical studies of water for hydrogen production due to the petroleum crisis [4], which also marks the beginning of the investigation into solar thermochemical conversion. During the solar thermochemical hydrogen production process, solar energy is concentrated to generate high temperatures so that water is split into hydrogen and oxygen [5]. However, this process requires a temperature as high as 2300 °C [6] and exceptional devices to separate hydrogen and oxygen from the mixture [7]. With the development of solar-concentrating technology and membrane technology, Abraham Kogan [8] proposed a porous ceramic membrane reactor, which added a

catalyst to water so that the water-splitting process could be carried out in multiple steps. Hydrogen and oxygen are generated in different reactions, avoiding the separation. At the same time, this process will lower the reaction temperature to below 1500°C. This process is the thermochemical cycle hydrogen production method. However, this method still has problems such as high reaction equilibrium temperature, which leads to increased heat conduction and heat radiation losses; and poor oxygen carrier kinetics, which leads to a long reaction cycle time. Consequently, researchers introduced carbon cycling, such as methanol steam reforming, to significantly reduce the reaction temperature. Yang [9] et al. reviewed the current methanol policy. The current methanol production route relies heavily on coal, ultimately increasing net greenhouse gas emissions and exacerbating coal market volatility, inconsistent with the carbon neutrality goals. With the widespread and large reserves of fossil raw materials, coal pyrolysis and gasification driven by solar energy have also attracted the attention of researchers. This chemical process is more mature than methane steam reforming and can realize the storage of solar energy and reduce CO_2 emission. Meanwhile, coal as a gasification feedstock has a syngas capacity of about 330 GWth, representing 76.7 % of all gasification feedstocks in the industry [10]. Thus, it has an irreplaceable role in producing fuels and chemical raw materials acting as a bridge for the transition from conventional to clean energy sources.

Solar concentrating technologies can generate a high temperature, which is especially suitable for coal gasification [11]. Researchers have investigated the solar coal gasification process on raw materials, reactors, and energy utilization forms. Gregg

et al. [12] studied solar coal gasification, using bituminous coal, activated carbon, coke, coal and biomass as raw materials, and estimated that about 60% of the solar energy entering the reactor was stored. Kodama et al. [13] conducted a high flux visible light coal gasification experiment in a small quartz reactor. They found that the fraction of incident light energy stored by CO is about 8%. Graggen [14] et al. designed an entrained-flow gasification reactor for gasification with a continuous stream vortex, resulting in an energy conversion efficiency of 9%. Weldekidan [15] et al. investigated different forms of concentrating technology in solar thermal conversion and believed that the parabolic disk form has the highest solar energy capture rate, with an optical efficiency of 94%. Wu [16] et al. proposed a dish system to collect solar energy to generate high-temperature steam, which acts as an agent to drive gasification. The primary energy efficiency reaches 51.34%. Generally, existing solar-driven coal gasification radiation forms mainly include direct radiation [17,18] and indirect radiation [19–21]. Direct radiation means that solar radiation directly enters the reactor through the quartz window and drives the gasification chemical process. Indirect radiation means that the solar is concentrated to heat the absorber and coal gasification is driven by thermal energy. Then the heat is transferred to the coal gasification reaction. Haftom [15] et al. analyzed these two energy utilization forms of carbon-based fuels. The study showed that the indirect radiation form can overcome the challenge of keeping the window clean. However, the heat transfer efficiency is lower than that of the direct radiation form. The concept of direct radiation bypasses the limitations imposed by conduction heat transfer through the ceramic walls, thus ensuring high

energy conversion efficiency. The main indicators of solar coal gasification performance: energy upgrade factor [20], that is, the ratio of the heat value of syngas to the heat value of raw materials, and energy conversion efficiency [22], that is, the ratio of the heat value of syngas and the sum of the heat value of solar energy and raw materials. Gokon [23] et al. investigated the coke gasification kinetic based on either the homogeneous or the shrinking core kinetic model and concluded that the form of circulation has a great influence on the conversion rate of gasification with the fluidized bed. Kodama [24] et al. studied the effects of metal oxides as filler materials on the kinetics of fluidized beds driven by solar energy. However, there is a lack of online thermogravimetric experimental data and a lack of kinetic and energy analysis of solar catalytic gasification. Mehrpooya [25] et al. studied the economics of solar-driven tube heat transfer and concluded that the use of nanofluids can significantly reduce the cost. Mousavi conducted the exergy analysis of the solar system. They obtained the trends in economics of exergy to months [26]and evaluated the life cycle of solar concentrating systems in remote areas[27]. Although exergy analysis of solar-driven power utilization systems has been studied, existing solar coal gasification research lacks kinetic and chemical process energy analysis based on experimental data. Thus, it is difficult to provide some guiding suggestions for actual industrial production. Meanwhile, there are few exergy analysis investigations on solar catalytic gasification systems with different solar irradiation.

In the industrial production of coal gasification, a high-temperature and high-pressure environment is required to achieve high conversion efficiency [28]. However,

it is difficult to maintain the high temperature and high-pressure gasification state. At the same time, it brings a significant economic burden to the investment and operation of equipment. As a third-generation coal gasification technology, adding a catalyst can reduce the reaction temperature by 200-300 K and achieve mild gasification under normal pressure. Besides, it can also significantly improve the gasification reaction rate and reduce energy consumption as well as equipment and materials requirements. It can directionally adjust the product gas composition, such as the amount of H_2 released [29,30]. It is known by researchers that K_2CO_3 and Na_2CO_3 have a strong catalytic effect on coal gasification. Kopyscinski et al. [31–33] found that K_2CO_3 could reduce the gasification temperature by 240 - 320 °C. The actual production of solar thermochemical conversion is greatly affected by uncontrollable factors. It is challenging to maintain a high-temperature state, and it is challenging to create high-pressure conditions. Therefore, the use of catalysts has a high practical value in the context of solar thermochemical conversion. Catalytic gasification is an important development field of solar coal chemical engineering. However, to the best of the authors' knowledge, there are currently few experimental studies on catalytic coal gasification with online thermodynamics analysis in solar thermochemical conversion.

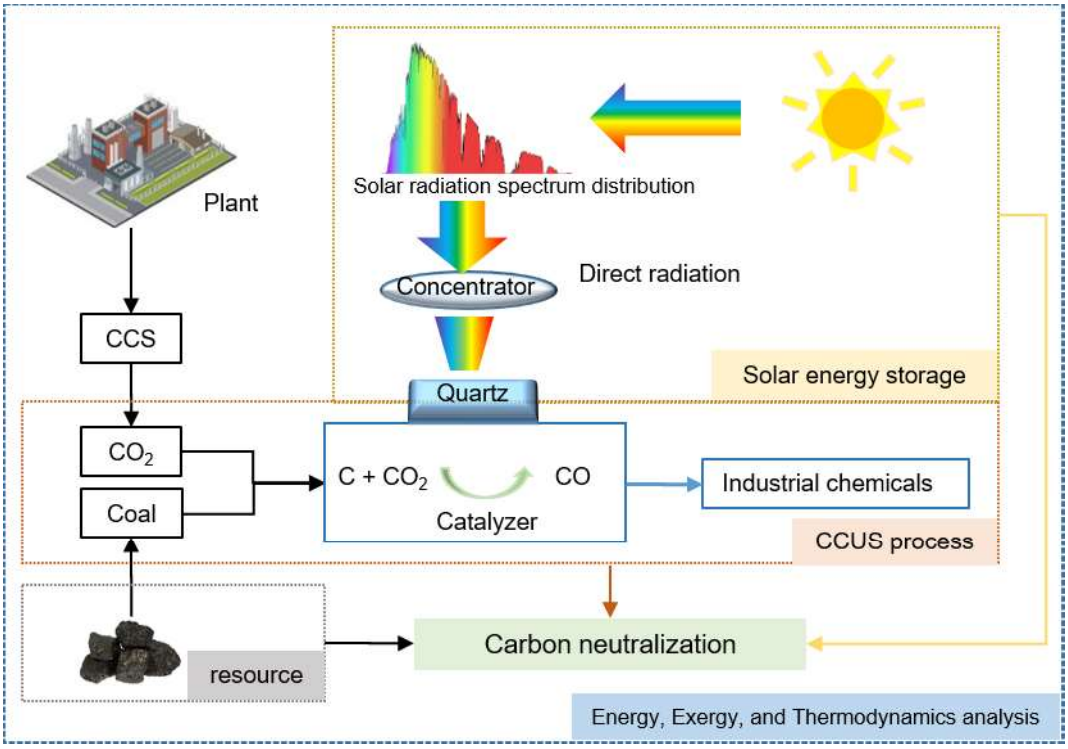

Figure 1 Carbon neutral solar coal gasification technology route

In this paper, a carbon-neutral solar coal gasification technology is proposed. Meanwhile, we independently design and develop a full-spectrum concentrated radiation-driven kinetic analysis test bench for investigating coal gasification reaction characteristics. This technology is based on solar energy to drive the coal gasification process, convert solar energy into fuel chemical energy to achieve solar energy storage, and realize coal resource utilization without combustion. The whole process is a low-carbon process. In addition, solar coal gasification processes using CO_2 captured by carbon capture and storage (CCS) technology as a gasification agent can be regarded as a Carbon Capture, Utilization, and Storage (CCUS) technology. Figure 1 shows that the coal gasification technology route based on concentrated solar-driven is comprehensively in line with the global demand for carbon neutrality. This route has a broad prospect and essential strategic value. Thermodynamic analysis of solar catalytic

gasification is an important part of the chemical process. The novelties of this research are as follows: (1) This work designed a novel experimental solar radiation gasification thermogravimetric device. (2) This work studied the gasification product distribution and the online kinetic analysis of different types and ratios of catalysts on experimental radiation gasification. (3) This work developed the energy and exergy analysis models based on experimental data for the solar gasification chemical process, which provides a reference for the engineering application of solar thermochemical conversion to chemical feedstock.

2 Experiment system and method

2.1 System setup

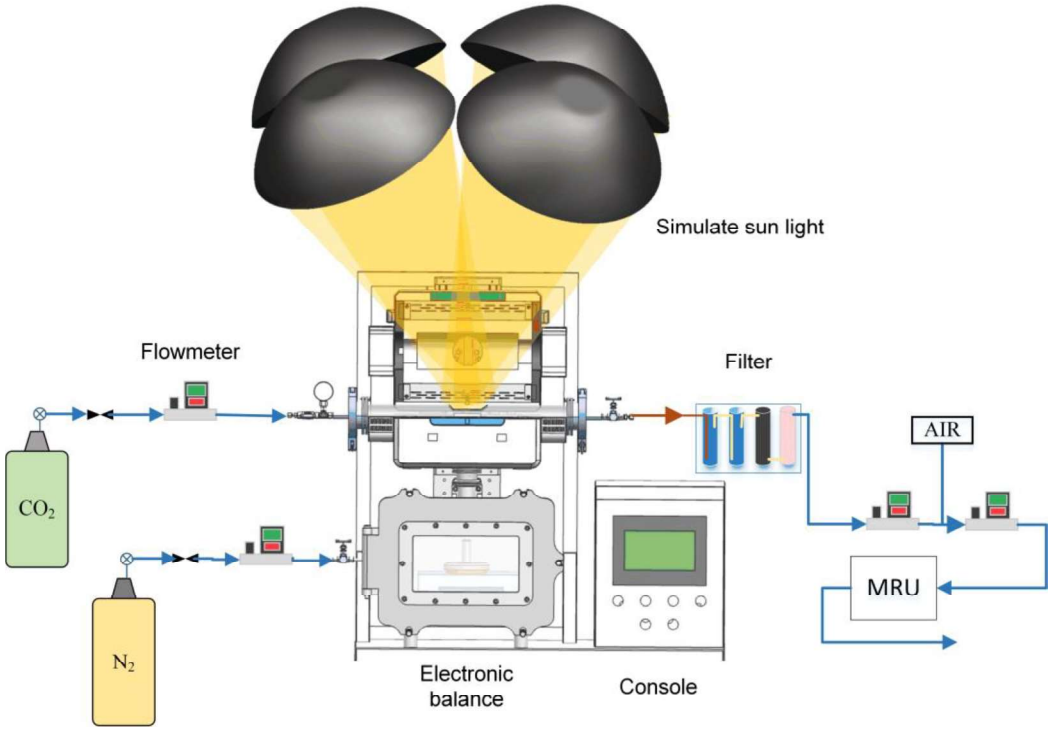

Figure 2 Schematics of the overall experimental setup

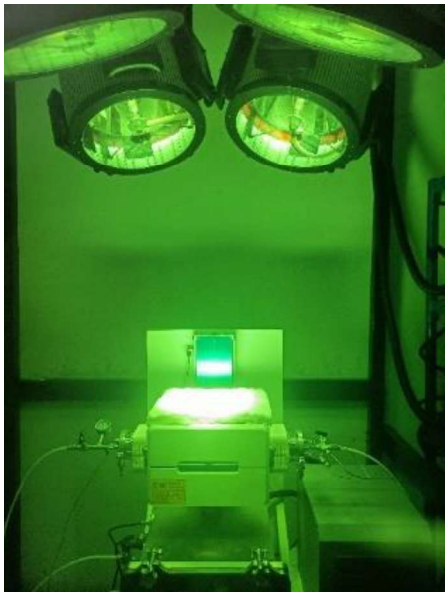

Figure 3 Radiation gasification system (photographed through a black glass sheet)

As shown in Figure 2, we designed and built our experimental setup based on the purpose of coal gasification under the full spectrum of concentrated solar. This setup consists of simulated sunlight, a coal gasification reactor, a thermogravimetric module, and an online flue gas analysis module. First of all, the simulated sunlight comprises four xenon lamps with a single electrical power rating of 0-7 kw, providing the approximate radiation flux of a concentrated solar energy system. The simulated light is adjusted to a spot size of 20 mm to cover the coal powder in the crucible completely. Figure 3 shows the state when running the experiment, where we shoot through the black glass sheet.

Secondly, the coal gasification reactor consists of a T-tube as the main body, which is connected to the thermogravimetric monitoring module underneath and the flue gas analysis module on the right. The coal is contained in a crucible held up by a quartz rod with a thermogravimetric monitoring module connected to the other end of the rod. CO_2 (purity above 99.95%) enters the gasification reactor through the left side of the T-tube.

184 N_2 (purity above 99.99%) enters the gasification reactor through the lower part of the
185 T-tube. It passes through and cools the thermogravimetric monitoring module during
186 the flow. In the reactor, we arranged four Omega type-k thermocouples to monitor the
187 temperature changes of the reaction process online. These locations include the quartz
188 tube irradiation surface, the right part of the T-tube, the crucible, and the insulation,
189 with details in Figure A1 of Appendix A. The gasification products flow to the flue gas
190 analysis module through the right side of the T-tube. Before entering the flue gas
191 analysis instrument (provided by German MRU), the flue gas is cooled and scrubbed
192 twice with pure water, then adsorbed and dried with graphite and SiO_2. Since the gas
193 flow rate is low, a certain amount of air is added in before entering the flue gas analyzer.
194 Finally, the excess gas is released into the vent. Among other things, details of the
195 reactor are in Appendix A.

196 Besides the information above, Hangzhou Jingong Special Company provides the
197 gas cylinder and pressure reducer. Alicat provides the flow meter. The Vario Plus gas
198 analyzer from MRU, Germany, analyzed the product gas components online, which can
199 determine the main components in the product gas, among which H_2 is determined by
200 thermal conductivity doppler (TCD), and the rest components are determined by the
201 non-dispersive infrared principle (NDIR).

202 2.2 Coal

203 The coal type selected for this study is provided by a subsidiary company of
204 Ningxia Coal Group in China. After receiving the coal, we ground, screened, and dried
205 it. The drying was done at 378 K for 12 hours. The coal used in the experiment was all

206 from the same batch.

207 Table 1 Main properties of the used coal

Proximate analysis (wt, ad, %)				Ultimate analysis (wt, ad, %)					$Q_{b,ad}$(MJ/kg)
M	V	FC	A	C	H	O	N	S	
4.15	26.63	59.58	9.64	68.58	3.86	12.40	0.80	0.57	26.66

208 Since there is no oxygen involved in the coal gasification process, the coal will
209 have two stages of endothermic reactions with temperature: pyrolysis and the
210 Boudouard reaction[34],

211 Pyrolysis:

212 $$\mathrm{Coal} \rightarrow \mathrm{C(s)} + \mathrm{CO} + \mathrm{H_2} + \mathrm{CH_4} + \mathrm{CO_2} + \mathrm{tar} + \mathrm{ash} \quad (1)$$

213 The Boudouard reaction：

214 $$\mathrm{C(s)} + \mathrm{CO_2} \rightarrow 2\mathrm{CO},\ \Delta H = 172.4\ \mathrm{kJ/mol} \quad (2)$$

215 2.3 Performance indicators

216 We quantify the radiation gasification performance based on three metrics to analyze
217 the experimental data. The first is the average carbon conversion rate, which is
218 expressed as:

219 $$\bar{X} = \frac{\int \dot{n}_{CO}dt + \int \dot{n}_{CO_2}dt + \int \dot{n}_{CH_4}dt - \int \dot{n}_{CO_{2,in}}dt}{n_{coal}} \quad (3)$$

220 where $\dot{n}_{CH_4}$, $\dot{n}_{CO_2}$, and $\dot{n}_{CO}$ are molar flow rates of CH_4, CO_2, and CO in the output
221 of T-tube, respectively, $\dot{n}_{CO_{2,in}}$ is the CO_2 molar flow rates in the input of T-tube. And
222 n_{coal} is the molar amount of coal fed into the reactor.

223 The second one is the ratio of the lower heating value (LHV) of product gas to the
224 LHV of coal, which is the energy upgrade factor, is expressed as:

$$U = \frac{\int \dot{n}_p LHV_p dt}{m_{coal} LHV_{coal}} \quad (4)$$

where $\dot{n}_p$ is molar flow rates of the product gas, m_{coal} is the mass of coal, LHV_p is the lower heating value of the product gas and the LHV_{coal} is the lower heating value of coal.

Last but not least, the third one is the energy conversion efficiency which is defined as the ratio of the sensible heat of insulation and the LHV of product gas to the sum of simulated solar lights and the LHV of coal, is expressed as:

$$\eta_{energy} = \frac{\int \dot{n}_p LHV_p dt + \int \dot{Q}_{insulation} dt}{\int \dot{Q}_{solar} dt + m_{coal} LHV_{coal}} \quad (5)$$

where $\dot{Q}_{insulation}$ is the sensible heat entering the insulation from the reactor in this setup, and $\dot{Q}_{solar}$ is the simulated solar power input to the reactor.

2.4 Dynamical analysis methods

Thermoanalytical kinetics is a method to study the rate and mechanism of chemical reactions, and the corresponding kinetic parameters can be obtained from kinetic reaction calculations. The gasification reaction in the reactor is a non-homogeneous reaction of solids, and according to the kinetic principle of thermal analysis, the reaction process can be expressed by the following equation

$$\frac{d\alpha}{dt} = f(\alpha) k(T) \quad (6)$$

where α is the conversion rate, t is the reaction time, $k(T)$ is the temperature dependence of the reaction rate constant, $f(\alpha)$ is the conversion function of the reaction.

According to the Arrhenius equation [35], the relationship between the reaction rate and temperature can be expressed as:

$$k(T) = A\exp(-\frac{E}{RT}) \quad (7)$$

where A is the pre-exponential factor, E is the activation energy, T is the reaction temperature, and R is the gas constant (8.314 $J \cdot K^{-1} \cdot mol^{-1}$). By combining eq. (6) and eq. (7), with adding the heating rate (coal gasification reaction is a non-isothermal process), $\beta = \frac{dT}{dt}$, to the combined equation, we can obtain the following equation:

$$\frac{d\alpha}{dt} = \frac{1}{\beta} A\exp(-\frac{E}{RT}) f(\alpha) \quad (8)$$

The single scanning rate method [36] calculates the kinetic parameters according to a non-isothermal thermogravimetric curve, which needs to assume the reaction conversion function. It is also called the hypothetical reaction model method. The widely used single scanning rate method is the Coats-Redfern method [37], which takes that the reaction conversion function is the reaction order model:

$$f(\alpha) = (1-\alpha)^n \quad (9)$$

where n is the order of the reaction.

Li [38] found that the gasification reaction of coal belongs to order one reaction, n = 1, so it can be obtained:

$$\ln\left[\frac{-\ln(1-\alpha)}{T^2}\right] = \ln\left[\frac{AR}{\beta E}\left(1-\frac{2RT}{E}\right)\right] - \frac{E}{RT} \quad (10)$$

In addition, for the activation energy at the general temperature of the gasification reaction, $\frac{E}{RT} \gg 1$, so, $1-\frac{2RT}{E} \approx 1$, substituting it into eq. (10),

$$\ln\left[\frac{-\ln(1-\alpha)}{T^2}\right] = \ln\frac{AR}{\beta E} - \frac{E}{RT} \quad (11)$$

Thus, we can take $\frac{1}{T}$ as the abscissa, and $\ln\left[\frac{-\ln(1-\alpha)}{T^2}\right]$ as the ordinate to plot a fitting line. Then we can calculate the activation energy under a specific heating rate. We optimize the process of the Coats-Redfern method by combining it with the

conversion of the reaction. The kinetic parameters are obtained by fitting within ± 50 K near a specific coal conversion.

2.5 Exergy analysis

To perform a technical evaluation of the hybrid system, we analyzed the exergy of the system. Exergy analysis combines chemical properties with system states (eg, temperature, pressure) to obtain overall exergy efficiency[39].

The solar exergy rate can be computed according to eq. (12) [26]：

$$\dot{E}x_{Sun} = A_d I_b[1 + \frac{1}{3}\left(\frac{T_{amb}}{T_{sun}}\right)^4 - \frac{4}{3}(\frac{T_{amb}}{T_{sun}})] \quad (12)$$

where A_d is the area of the concentrator, I_b is expressed as solar irradiance. T_{amb} and T_{sun} imply to the ambient temperature (details are in Appendix B) and sun temperature (5600 K) respectively.

Meanwhile, the exergy loss including heat transfer, convection, and radiation losses from the solar dish module can be calculated according to eq. (13) [26]：

$$\dot{E}x_{L,Dish} = (1 - \frac{T_{amb}}{T_{gasifier}})\dot{Q}_{L,dish} \quad (13)$$

where $T_{gasifier}$ is the reaction temperature of the gasifier, and $\dot{Q}_{L,dish}$ is expressed as heat loss of solar dish module (details are in Appendix B eq. (B4) to eq. (B13)).

The exergy efficiency of the solar dish module can be formed as follows [40]:

$$\psi_{E,dish} = \frac{P_{dish} - \dot{E}x_{L,Dish}}{\dot{E}x_{Sun}} \quad (14)$$

where P_{dish} implies output power of solar dish module (W).

The state of the coal entering the gasifier is close to the dead state. Thus, the physical exergy of the coal is considered zero. The chemical exergy of the fuel can be computed according to eq. (15) [41]：

$$\dot{E}x_{C,coal} = \dot{m}_{coal} e^{C}_{coal} \quad (15)$$

$$e^{C}_{coal} = LHV[1.0064 + 0.1519\frac{H}{C} + 0.0616\frac{O}{C} + 0.0429\frac{N}{C}] \quad (16)$$

where $\dot{m}_{coal}$ (kg/s) and e^{C}_{coal} (J/g) belong to the fuel mass flow and specific chemical exergy. H, C, O, N is expressed as the mass fraction of elements (details are in Table 1).

The exergy efficiency of the gasifier module can be formed as follows[42]:

$$\psi_{E,gasifier} = \frac{P_{product}}{\dot{E}x_{C,coal}} \quad (17)$$

where $P_{product}$ implies the exergy of gasification products.

The exergy efficiency of the solar coal gasification system can be computed according to eq. (18):

$$\psi_{E,system} = \frac{P_{dish}+P_{product}}{\dot{E}x_{Sun}+\dot{E}x_{C,coal}} \quad (18)$$

This study evaluates the solar coal gasification system with experimental thermodynamics, energy models, and exergy analyses to guide industrial production. The thermodynamic, energy and exergy models used in this study were calculated with homemade MATLAB programs.

2.6 Operational details

Gasification requires a high temperature. We have selected various operating conditions, as shown in Table 2, to ensure that the gasification reaction is thorough enough; and to reduce the temperature drop from the excessive convection heat transfer caused by high-speed flow. Comparing Case 1 and Case 2 reveals the effect of catalyst addition on indirect radiation gasification while comparing Case 1 and Case 3 is to study the differences in radiation forms. Furthermore, comparing Case 4, Case 5, and Case 6 is to study the effect of the ratio of catalysts under direct radiation. And

313 comparing Case 5 and Case 7 is to investigate the effect of catalyst types. *R* is the ratio
314 of catalyst to coal. The experimental mix form is physically mixing.

315 Table 2 Experimental parameters of the solar-driven coal gasification

Case	radiation form	Coal (g)	CO_2(L/min)	N_2(L/min)	Catalyst		*R*
					K_2CO_3(g)	Na_2CO_3(g)	
Case 1	indirect	1	0.05	0.075	0	0	0
Case 2	indirect	1	0.05	0.075	0.1	0	0.1
Case 3	direct	1	0.05	0.075	0	0	0
Case 4	direct	1	0.05	0.075	0.05	0	0.05
Case 5	direct	1	0.05	0.075	0.1	0	0.1
Case 6	direct	1	0.05	0.075	0.2	0	0.2
Case 7	direct	1	0.05	0.075	0	0.05	0.05

316

317 3 Results and discussion

318 3.1 Comparison of direct and indirect radiation gasification

319 N_2 and CO_2 were used to purge the reactor. We started the experiment when the gas
320 components were kept within ±0.1% fluctuations for 10 minutes. We turned on a
321 simulated light at 5 mins intervals during the experimental operation.

322

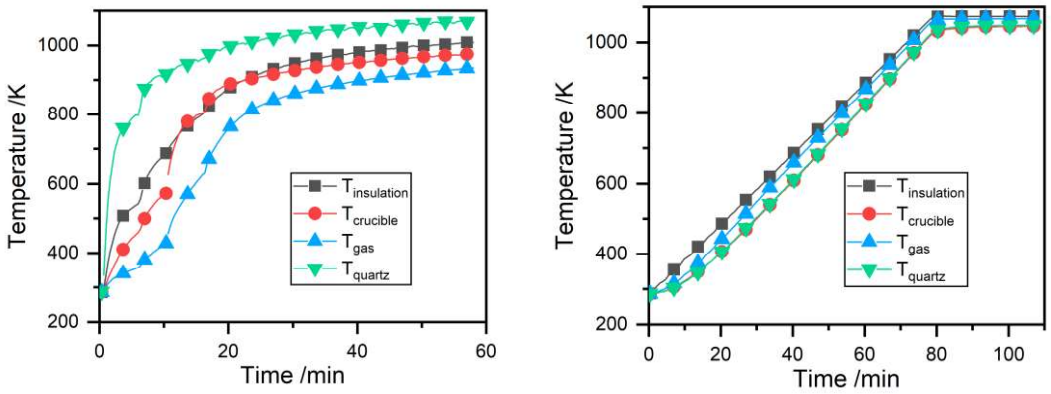

(a) Direct radiation gasification (b) Indirect radiation gasification

Figure 4 Time evolution of temperature

Figure 4 (a) shows the time evolution of the temperature measured by the four Omega k-type thermocouples. The temperature of the quartz tube is always the highest, and the gas temperature is always the lowest. The maximum temperature difference between the two is nearly 400 K. With the advance of time, the temperature of the crucible is first lower than that of the insulation, reaching the same in about 18 minutes, and finally, the two tend to be close.

We use resistance wire heating to simulate indirect radiation gasification. Fig. 4 (b) shows the time evolution of temperature under indirect radiation gasification. The location of the four thermocouples is the same as that of the direct radiation gasification system, but their change trend is different. It can be seen that the difference between the four temperature curves is smaller than that of the direct radiation gasification system. The maximum temperature difference of the four thermocouples at the same time point is about 50 K. Besides, the temperature change trend measured by the four thermocouples is the same, reaching a constant set temperature of 1073 K at the set time.

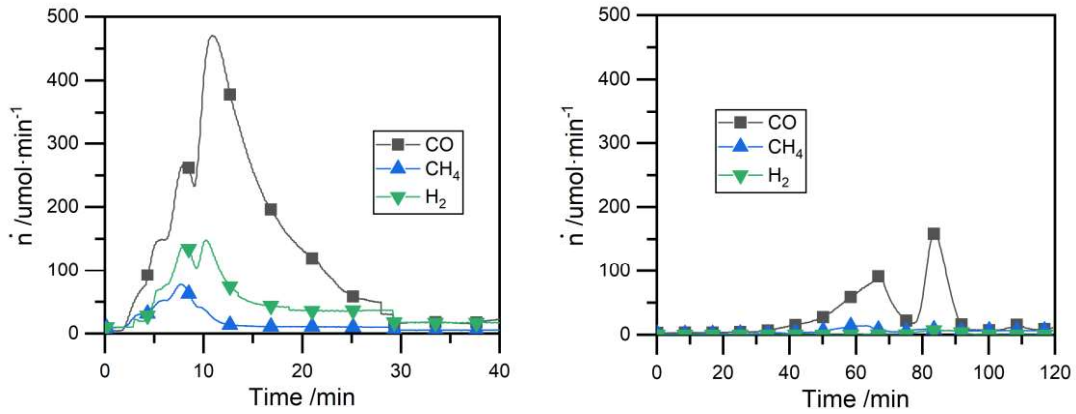

(a) Direct radiation gasification (b) Indirect radiation gasification

Figure 5 Time evolution of molar flow rates

Figure 5 shows the time evolution of products of gas. The gas production rate of the radiation gasification system is the focus of system product analysis. The gasification reaction process of direct radiation and indirect radiation is different. On the one hand, there will be light and heat synergy under the spotlight of four xenon simulated lights for direct radiation gasification. Comparing Fig. 5 (a) and Fig. 5 (b), the time point of the carbon monoxide production of direct radiation gasification is earlier than that of indirect radiation gasification. Moreover, at the same reaction temperature, the amount of carbon monoxide obtained by direct radiation gasification is much higher than that of indirect radiation gasification. There is only one peak under direct radiation gasification from the peak distribution of product gas rate in the reaction process. Komada [13] et al. reported the same distribution under direct radiation gasification.

On the other hand, the coal pyrolysis and the Boudouard reaction under indirect radiation gasification have an apparent time order. Sanchez-Hervas [43] et al. reported that when the temperature reaches about 500 ℃, coal begins to experience pyrolysis, and the carbon monoxide product belongs to the volatile. When the temperature reaches 650 ℃, the coal char reacts with CO_2 and generates more carbon monoxide. This trend

354 is consistent with the experimental results in Fig. 6 (b).

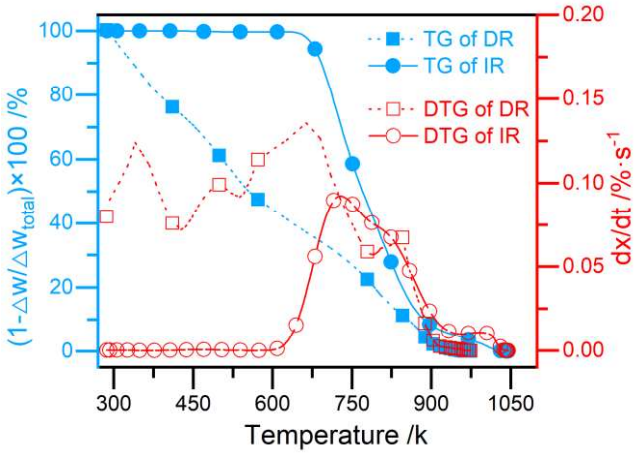

355

356 Figure 6 Reactivity of coal in different radiation forms

357 Figure 6 shows the reactivity of coal under direct radiation (DR) and indirect (IR)
358 radiation based on the thermogravimetric (TG) and differential thermogravimetric
359 (DTG) analysis. It can be seen that the TG curve shifts toward the high-temperature
360 region during indirect radiation and the peak of the DTG curve decreased by 34%.
361 These results indicate that the coal reactivity under indirect radiation is lower than that
362 under direct radiation. This is mainly because the process of devolatilization under
363 indirect radiation gasification is slower, and more volatile components are attached to
364 the coal char surface[44]. The residual volatiles are further removed, and the difference
365 in coal reactivity under indirect and direct radiation becomes smaller with temperature.
366 At the same time, the molecular structure of coal char shifts towards graphitic crystals
367 with temperature, which leads to a decrease in reactivity.

368 3.2 Effects of catalyst types under direct radiation gasification

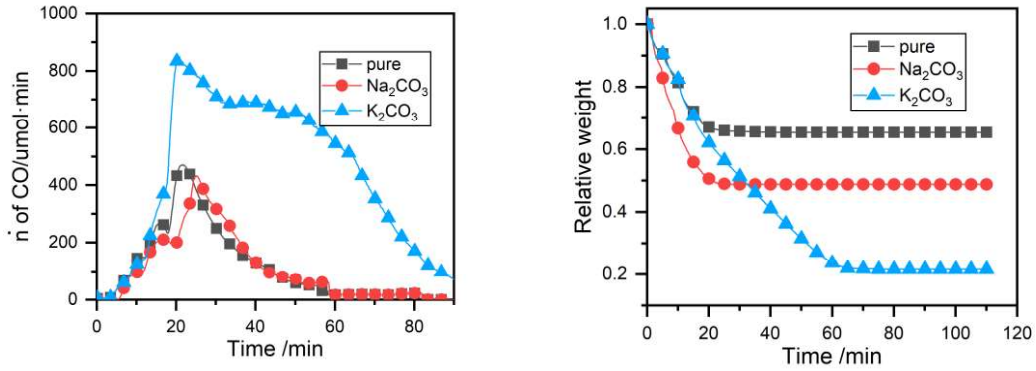

(a) Time evolution of CO molar flow rates

(b) Time evolution of weight loss

Figure 7 Direct radiation gasification characteristics of different catalysts

Fig. 7 (b) shows that radiation gasification cannot reach a high conversion under this temperature (1073.15 K). The means to increase the conversion are high pressure or catalysis. We usually choose to add appropriate catalysts under laboratory conditions. We selected two common catalysts for coal gasification, Na_2CO_3, and K_2CO_3. Fig. 7 (a) shows that the molar flow rate of CO after adding Na_2CO_3 is consistent with the direct radiation gasification without adding any catalyst and reaches the peak at almost the same time point. At the same time, Fig. 7 (b) shows that the conversion rate after adding Na_2CO_3 is higher than that without adding any catalyst, which is about 20%. These results show that the catalytic effect of Na_2CO_3 on the Boudouard reaction is poor in the form of direct radiation gasification at this temperature.

However, the situation is different with K_2CO_3 added. Fig. 7 (a) shows that the peak value of CO molar flow rate with K_2CO_3 is about twice that of the other two groups. Meanwhile, the conversion rate after adding K_2CO_3 is the highest. Thus, we used K_2CO_3 as the catalyst for direct radiation gasification in subsequent experiments.

3.3 Effects of K_2CO_3 on direct or indirect radiation gasification

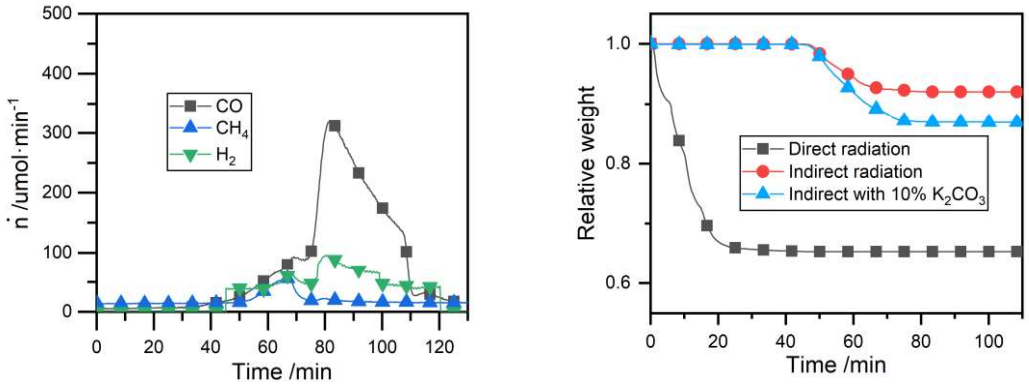

(a) Time evolution of CO production rate (indirect radiation with K_2CO_3)

(b) Time evolution of weight loss

Figure 8 Gasification characteristics of different radiation forms

We also investigate the addition of K_2CO_3 under indirect radiation gasification. The effects of K_2CO_3 and radiation form (direct or indirect radiation) on gasification are compared in the subsequent analysis. Fig. 8 (a) shows the time evolution of gas product rates under indirect radiation with K_2CO_3. Compared to Fig. 5 (b), there is only one peak in CO molar flow rate. This is because the gasification reactivity is strengthened under the catalysis of K^+, and the Boudouard reaction of coal char begins at a lower temperature[32].

However, Fig. 8 (b) shows direct, indirect, and indirect catalytic radiation gasification weight loss. We found that the catalyst can enhance the reactivity of coal gasification and improve coal conversion to a certain extent, but this improvement is limited on indirect radiation form. In Fig. 8 (b), although direct radiation can enhance the reactivity of gasification, the weight loss rate can be further improved. Meanwhile, in Fig. 7 (b), the weight loss rate sees a big increase with the addition of catalyzes on direct radiation form. Therefore, we will add catalysts under direct radiation gasification in the follow-up research. The product's production rate under direct

radiation with K_2CO_3 would be present in the next section.

3.4 Effects of different catalyst ratios on gasification reaction under direct radiation

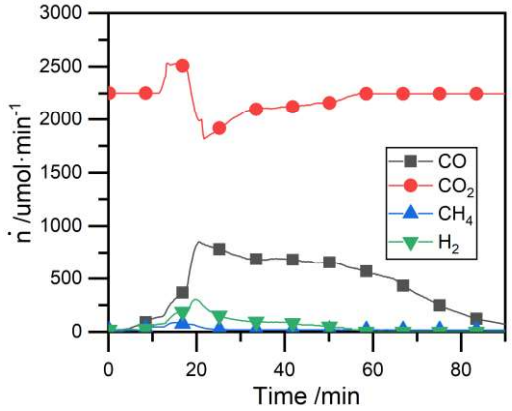

(a) Molar flow rates of the gas in Case 4 (5 % K_2CO_3)

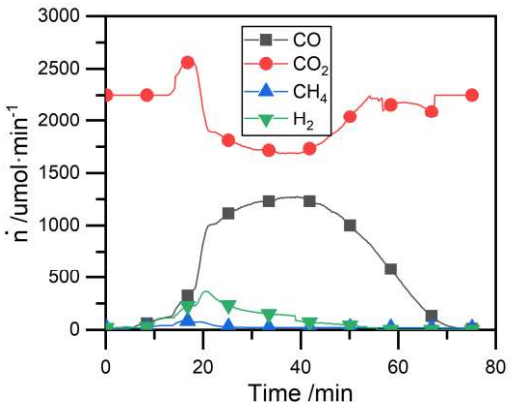

(b) Molar flow rates of the gas in Case 5 (10 % K_2CO_3)

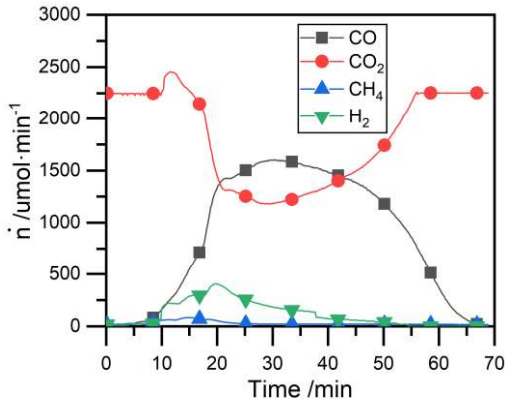

(c) Molar flow rates of the gas in Case 6 (20 % K_2CO_3)

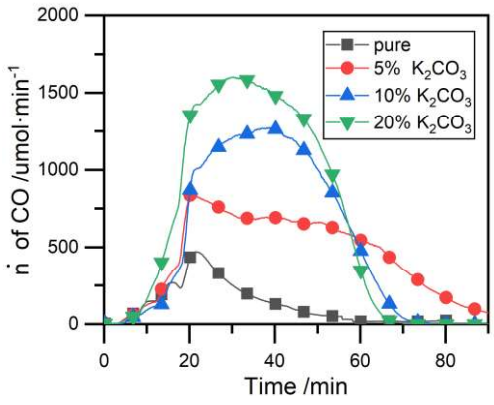

(d) Molar flow rates of CO in cases 3, 4, 5, and 6.

Figure 9 Molar flow rates of the cold product gas in different proportions of catalyst

We investigated the influence of different K_2CO_3 ratios (5%, 10%, and 20%) on gasification distribution. Figure 9 shows the mole flow rates of the gas products in different ratios and the CO molar flow rates comparison of four cases. As shown in Fig. 9 (a), the molar flow rate of CO_2 increases with temperature, marking the beginning of pyrolysis. And the peak value of CO_2 reached about 2500 umol/min with the progress of primary pyrolysis. Then, the gasification reaction (the Boudouard reaction) begins

with the decrease of CO_2, and CO starts to generate, with a peak value of about 800 umol/min. With the progress of the reaction, the coal char is subject to secondary pyrolysis, and the end sign is that the generation of H_2 stops. Fig. 9 (b) shows that the decrease of CO_2 increases with the ratio of K_2CO_3, indicating the rise in the gasification reaction rate. The rate curves of CO_2 and CO intersect in Fig. 9 (c), which means the Boudouard reaction is more intense. Fig. 9 (d) shows that the molar flow rate of CO increases with the addition and ratios of K_2CO_3, and the peak generation rate increases from about 500 umol/min without a catalyst to about 800 umol/min (5 % K_2CO_3), then to about 1650 umol / min (20 % K_2CO_3). The catalytic effect is pronounced. However, the increase in peak value decreases with the ratio of K_2CO_3, which is the same trend as the gasification study of Jan et al. [31]. With the massive use of CO2, the solar gasification system produces chemical feedstocks. This process realizes the low carbon use of coal resources.

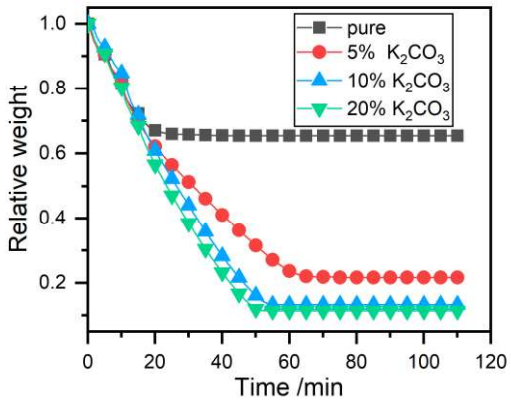

Figure 10 Time evolution of weight loss with different K_2CO_3 ratios

Figure 10 shows the time evolution of different relative weight K_2CO_3 ratios. In combination with the results in Fig. 9 (d) and Fig. 10, the addition of K_2CO_3 can make the Boudouard reaction more thorough and the coal conversion higher. The addition of

catalyst also leads to the Boudouard reaction taking longer than non-K_2CO_3. However, the catalysis Boudouard reaction time is shortened by about 20 mins with K_2CO_3 ratios increase. Comparing the thermogravimetric and molar flow rates of CO in Fig. 9 (d) and Fig. 10, 20 % K_2CO_3 can only improve a few compared to 10 % K_2CO_3. These results mean that 10 % K_2CO_3 can make gasification thorough.

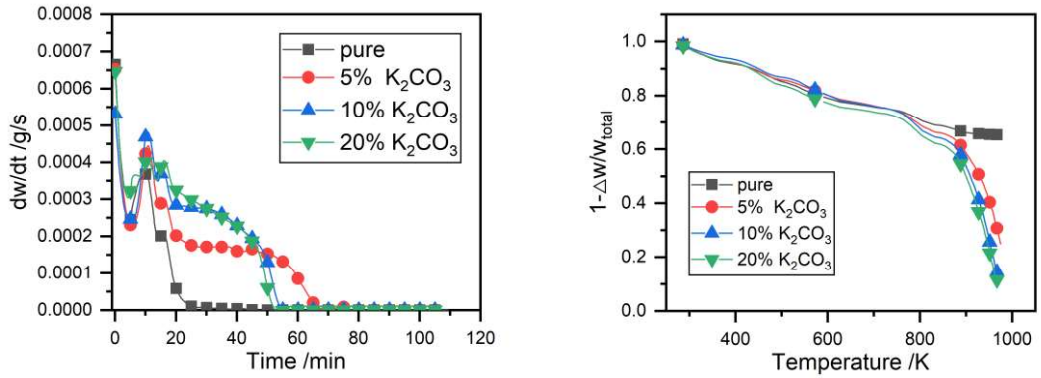

(a) Time evolution of weight loss rates (b) Temperature evolution of weight

Figure 11 Kinetic with different K_2CO_3 ratios

Fig. 11 (a) shows the time evolution of weight loss rates with different K_2CO_3 ratios. All four curves see decreases immediately at the beginning of the devolatilization reaction. After removing volatiles, CO_2 enters the coal char particles for a gas-solid two-phase reaction. The progress of the Boudouard reaction will lead to the consumption of the solid components of the coal char and expose more pores in the coal char. The gas-solid contact area increases with pore size, and the specific surface area of the Boudouard reaction increases. Therefore, the weight loss rate increases at this stage. When the Boudouard reaction proceeds to a certain extent, the consumption of coal char substantially decreases, and the gas-solid contact area decreases gradually. The specific surface area and reaction rate of the Boudouard reaction are reduced with the crosslinking or collapse of the pore structure in the coal char. Besides that, K_2CO_3

has no catalytic effect on the devolatilization reaction. Sharma[45] et al.investigated the relationship between coal gasification reactivity and catalyst addition. The experimental results show that the gasification reactivity of coal char increases with catalyst addition, but there is an optimal addition. When the optimum addition amount is higher than that, the activity of the excess catalyst decreases because their mutual accumulation will increase the average particle size of coal char but reduce the contact area of the coal char surface.

Fig. 11 (b) shows the temperature evolution of weight loss with different K_2CO_3 ratios. When the temperature reaches 750 K, the decreasing slopes of the four curves increase—the gasification reaction stage at this temperature. The pure coal curve has a minor descending slope and the smallest descending magnitude. However, direct radiation catalytic gasification is remarkable. As the catalyst addition ratio increased from 5% to 10%, the volume of the decrease also increased. However, the improvement was limited when the catalyst ratio was increased from 10% to 20%. At the same time, we can also see from Fig. 11 (b) that the separate temperature between the pure curve and the others is about 900 K, which indicates that the K_2CO_3 starts to catalyze at about 900 K.

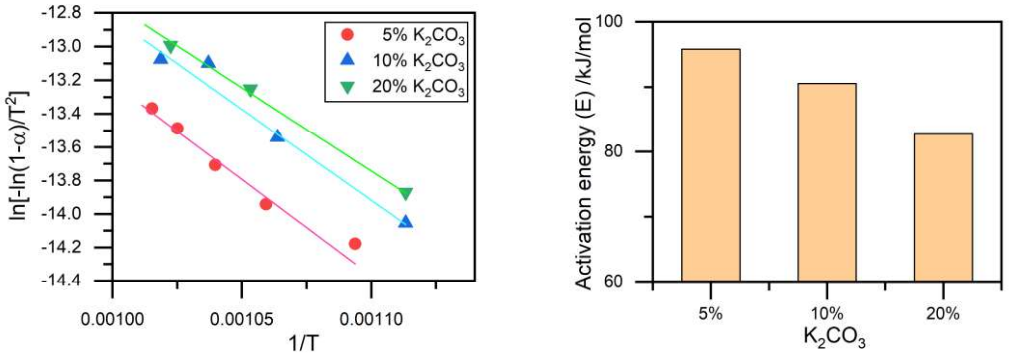

(a) Arrhenius plot (b) Comparison of different ratios

Figure 12 Kinetics analysis at cases 4, 5, and 6

460 Figure 12 shows kinetic analysis using the Coats-Redfern method for different
461 catalyst ratios (5%, 10%, and 20%) of direct radiation catalytic gasification. Fig. 12 (a)
462 shows the fitting Arrhenius plot for cases 4, 5, and 6. The activation energy obtained is
463 95.81 kJ/mol, 90.54 kJ/mol, and 82.86 kJ/mol in Fig. 12 (b).

464 In the initial reaction stage, the temperature is low, but the heating rate is high, and
465 the volatiles will be rapidly removed. During the second half of the reaction, the coal
466 char and catalyst undergo the typical behavior of pore development during coke
467 conversion, which can lead to higher surface area and faster rates. And the activation
468 energy decreases with the catalyst ratio. At higher conversion rates, the gasification rate
469 decreases due to pore collapse and larger potassium clusters. The latter is formed as the
470 surface carbon is released as carbon monoxide gas, and the amount of potassium
471 relative to the carbon increases. The release of residual volatiles, the diffusion of
472 reactive gases, and the expansion of porosity in the coal char all affect the activation
473 energy distribution of gasification.

474 4 Analysis of radiation gasification performance indicators

475 4.1 Element C conversion rate

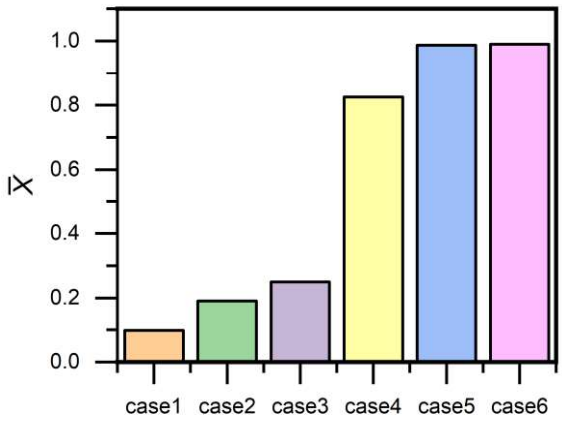

Figure 13 Distribution of elemental C conversion rate

As shown in Fig. 13, we investigate the conversion degree of the coal during radiation gasification by the conversion rate of the C element. The conversion rate of the C element in Case 1 is 0.098. And the conversion rate of Case 3 is 0.25, which is about 2.5 times that of Case 1. The catalyst further improved the C element conversion rates, and the rates of cases 4-6 were 0.825, 0.987, and 0.99, respectively. Case 2 is indirect radiation catalytic gasification, but it is only 0.19. These results show that direct radiation is more effective. The introduction of catalyst alone cannot directly improve the conversion of C element with indirect radiation. The synergistic effect of light and catalyst can significantly improve the conversion of the C element at this temperature.

4.2 Energy conversion efficiency

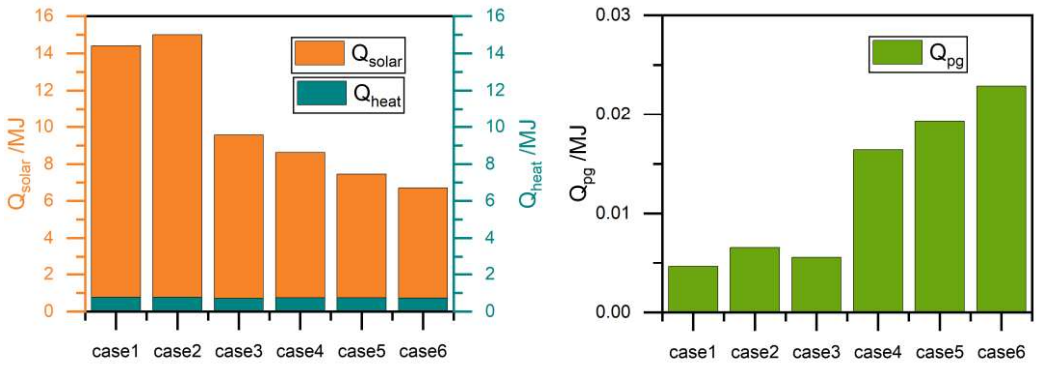

Figure 14 (a) Solar energy and sensible heat

Figure 14 (b) The heat value of the product gas

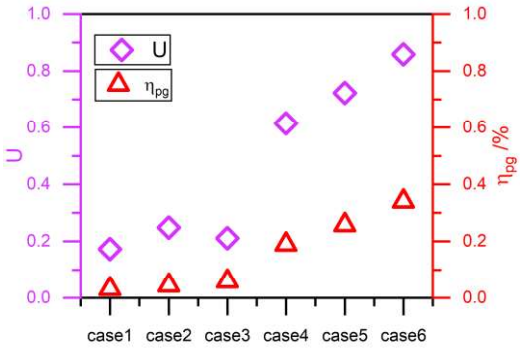

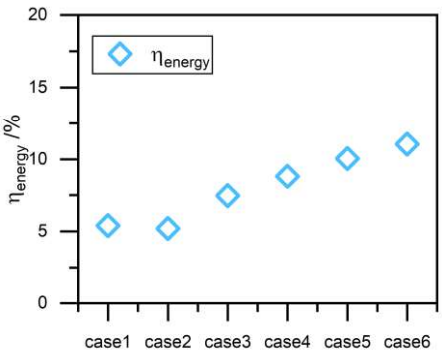

Figure 14 (c) U and η_{pg}

Figure 14 (d) Energy conversion efficiency

Figure 14 System energy distribution

Figure 14 shows the radiant gasification system's energy, including the insulation's sensible heat (Q_{heat}), the heat value of the product gas (Q_{pg}), and the input solar energy (Q_{solar}). At the same time, we calculated energy conversion efficiency (η_{energy}), product gas energy efficiency (η_{pg}) and energy upgrade factor (U).

Indirect radiation gasification (Case 1 and Case 2) requires more solar energy due to its long reaction time. The reaction time for direct radiation gasification is shortened with the catalyst addition. The required solar energy input is also reduced to 6.25 MJ in Figure 14 (a). The catalyst can improve Q_{pg} of indirect radiation gasification (Case 2), but under the synergistic effect of direct radiation (Case 5), Q_{pg} will see a significant increase, about three times that of Case 2 in Figure 14 (b). For Q_{heat}, the temperature rises of each working condition are the same, and there is little difference.

The solar system efficiency under direct radiation gasification will increase from 5.39 % (Case 1) to 7.47 % (Case 3) in Figure 14 (d). The addition of catalysts will further advance this trend, reaching a maximum level of 11%. The trend of product gas

503 efficiency is similar to solar system efficiency, which is also greatly improved by the
504 synergistic effect of direct radiation and catalyst. Compared with the conversion rate of
505 the C element, the energy upgrade factor is to analyze the radiation gasification system
506 from the perspective of energy. Adding a catalyst can improve the energy upgrade factor
507 of indirect radiation gasification. Direct radiation gasification can also enhance the
508 energy upgrade factor, which indicates that radiation's incoming form will affect energy
509 absorption and utilization. At the same time, in the form of direct radiation, the addition
510 of a catalyst can significantly improve the energy upgrade factor. Moreover, the
511 increase ratio is proportional to the ratio of catalyst, and the highest can reach about
512 0.86 in Figure 14 (c). The data in Figure 14 are only for the analysis of the experimental
513 process and evaluation. The solar energy entering the gasifier is converted into forms
514 such as chemical energy, which is the storage process of solar gasification. This process
515 is an important means of low carbon use of coal resources.

516 5 Chemical process analysis

517 5.1 Energy analysis

518 We set up three model forms: indirect radiation, direct radiation, and direct catalytic
519 radiation gasification, to investigate the feasibility of applying solar heat sources in the
520 actual coal gasification chemical process. In the actual process, the forms of solar
521 energy utilization include tower type, trough type, and dish type. For the coal
522 gasification chemical process, the disc type has the advantages of flexible installation,
523 concentrated light spot energy, and high temperature, convenient for installation in
524 various terrain. Therefore, we use the dish type to collect and utilize solar energy and

analyze the chemical process energy and exergy. For the whole system, we consider the energy loss of each part. See the calculation process in Appendix B for details. At the same time, we use the corresponding experimental conditions for different systems to predict the product distribution and then carry out the model calculation of coal gasification reaction. At the same time, we compare the overall efficiency of the three systems and the receiver dish area of the disc system.

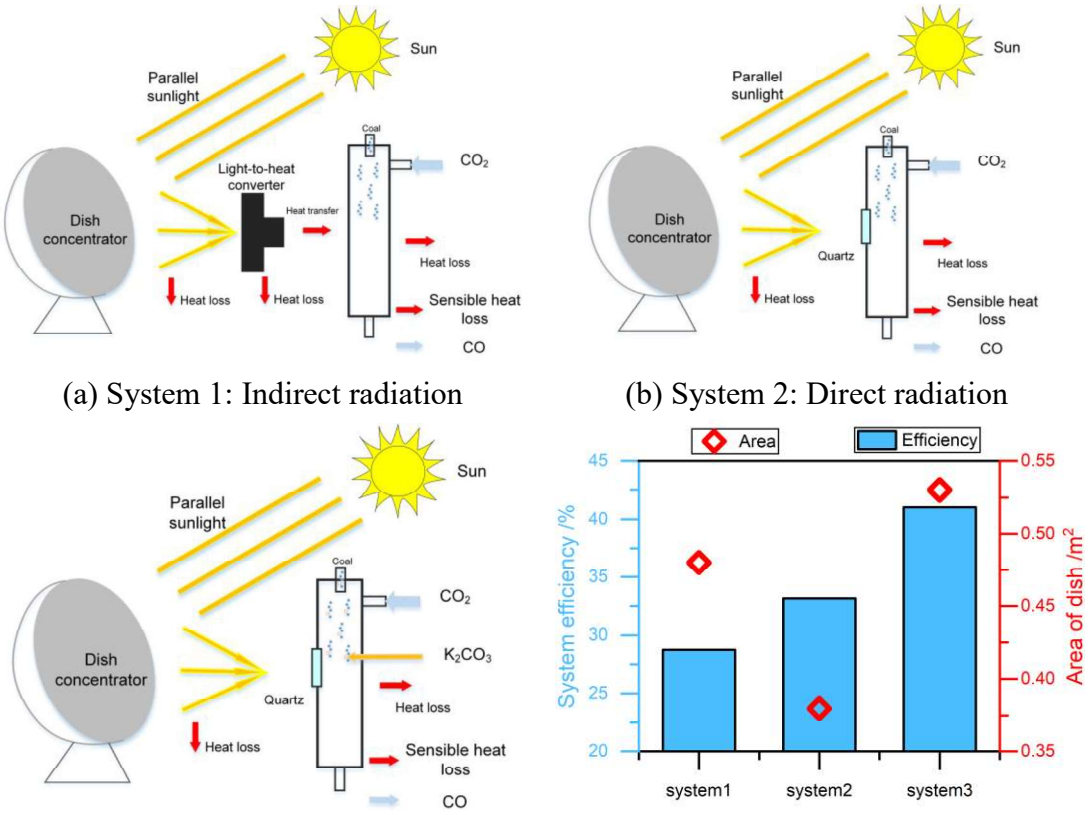

(a) System 1: Indirect radiation (b) System 2: Direct radiation

(c) System 3: Direct catalytic radiation (d) Systems comparison

Figure 15 Different solar energy coal gasification systems

Table 3 Experimental gas products distribution

Products	Volume distribution (%)			Mass distribution (%)		
	System 1	System 2	System 3	System 1	System 2	System 3
CO	68.16	56.22	68.74	66.60	66.73	70.22
CH_4	12.68	7.64	2.30	7.08	5.19	1.34
H_2	2.12	22.08	11.77	0.15	1.87	0.859
CO2	17.04	14.05	17.19	26.17	26.21	27.58

Fig. 15 shows three radiation coal gasification systems and their comparison.

According to the experimental data above, the gas product distribution is in Table 3. For System 1, the heat loss from the concentrator to the reactor was considered. The input coal rate is 135.05 g/h (1 kW heat value). With the same gasification agent and coal ratio as the experiment, the flow rate of CO_2 is 405 L/ h, and the flow rate of N_2 is 607.5 L/h. Estimate the sensible heat loss carried by gases at 800 ℃, referring to the heat value of various gases in [46]. The heat at the reactor output is expressed as

$$\dot{Q}_{output} = \dot{Q}_{sensible} + \dot{Q}_{pg} \quad (19)$$

where $\dot{Q}_{output}$ is the output total heat rate, $\dot{Q}_{sensible}$ is the sensible heat rate, and $\dot{Q}_{pg}$ is the low heat value rate of gas products.

(a) First of all, in System 1:

$$\dot{Q}_{output} = 492.32 \text{ W}$$

The heat rate required by the gasifier is

$$\dot{Q}_{gasifier} = \dot{Q}_{output} + \dot{Q}_{wall} \quad (20)$$

where $\dot{Q}_{wall}$ is the heat loss through the wall, and it is 1.7% of $\dot{Q}_{coal}$ [47]. Then reverse the solar input energy. The system efficiency can be expressed as follows:

$$\eta_{system} = \frac{\dot{m}_p LHV_p}{\dot{Q}_{solar} + \dot{m}_{coal} LHV_{coal}} \quad (21)$$

The efficiency from obtaining solar energy to input energy into the reactor (η_{SE}) is 75.31 %, the system efficiency (η_{system}) is 28.76 %, and the dish area (s) is 0.48 m^2.

(b) Secondly, in System 2:

There is no converter in System 2. Thus, the energy calculation does not consider the converter's transfer and radiation energy loss. We assume that the absorption coefficient of coal is 0.9. We think that the temperature in the reactor is the same as in System 1.

$$\dot{Q}_{output} = 522.77 \text{ W}$$

The system efficiency (η_{system}) is 33.15 %, and the dish area (s) is 0.38 m^2.

(c) Last but not least, in System 3:

The gasification in System 3 is direct radiation with K_2CO_3 addition.

$$\dot{Q}_{output} = 723.58\ W$$

The system efficiency (η_{system}) is 41.04 %, and the dish area (s) is 0.53 m^2.

Fig. 15 (d) compares three different systems on efficiency and the dish area. Under the premise of ensuring the same reactor temperature, direct radiant gasification can obtain higher system energy conversion efficiency. Simultaneously, adding a catalyst can further increase this advantage. Industrial production is often accompanied by large-scale production. Considering the economics of construction, the area of the dish is an important reference indicator. Compared with System 1 and System 3, the dish diameter increases by 5 %, but the efficiency increases by 13 %. The greatly improved system efficiency can further enhance the economic benefits of the large-scale chemical process.

5.2 Exergy analysis

This work investigates the exergy analysis in the solar gasification chemical process, which include the solar concentrator, coal gasifier, and the whole system. The exergy efficiency of different modules provides a reference for the solar gasification chemical process.

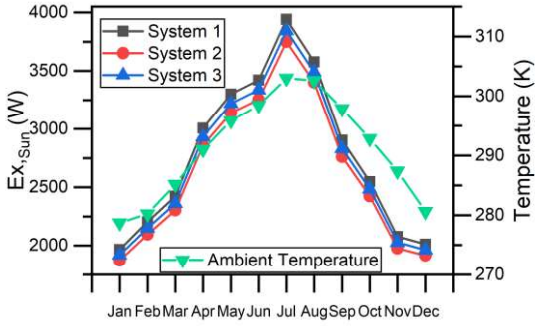

(a) The monthly evolution of the solar exergy and ambient temperature

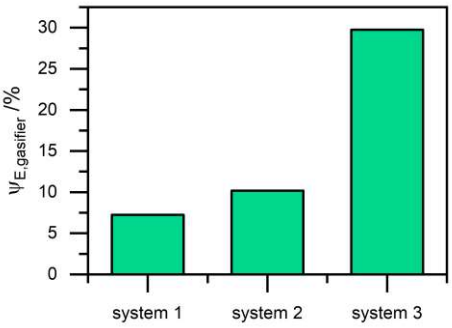

(b) The gasifier exergy efficiency of different systems

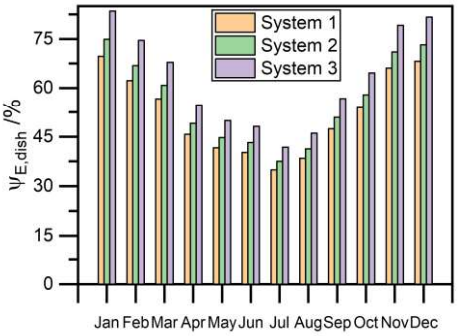

(c) The monthly evolution of the solar dish exergy efficiency

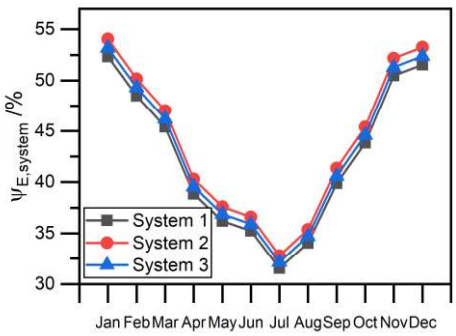

(d) The monthly evolution of system exergy efficiency

Figure 16 The module exergy analysis results

Fig. 16 (a) shows the monthly evolution of solar dish module exergy analysis and ambient temperature[48]. The solar dish module exergy relates to the ambient temperature. It reaches its peak in summer (3941.18 W/m^2), and the least value of exergy content belongs in December (1871.57 W/m^2). This trend is similar to the solar power module in Ref. [26]. The areas of different systems in the exergy analysis are calculated in Section 5.1 which meets the thermal power needed by the gasifier. The area of the solar dish influences the solar exergy according to eq. (12). The value of solar exergy in system 1 is the highest, as well as that in system 2, which is the least due to different dish areas in the same month. Fig. 16 (b) shows the gasifier exergy efficiency in different systems. The gasifier exergy efficiencies are influenced by the

product distribution and gasification efficiency. It can be concluded that the highest amount of gasifier exergy efficiency belongs to the direct catalytic radiation gasification (system 3, 29.7 %). Fig. 16 (c) shows the monthly evolution of the solar dish exergy efficiency. It can be seen that exergy efficiency decreases with an increase in thermal losses. This law is in good agreement with the values reported in Ref [49]. Fig. 16 (c) also shows that the chemical process of solar gasification needs to be considered with the impact of seasons. This chemical process includes not only the influence of reaction temperature but also the influence of ambient temperature with effects on the exergy efficiency of solar modules. For any month, System 3 always had the highest exergy efficiency of solar modules.

Fig. 16 (d) shows the monthly evolution of the system exergy efficiency in different solar gasification systems, the trend of which is similar to the study [26]. The reason for the decrease in summer is the increase in entropy caused by higher temperature, but the gasifier exergy remains unchanged, resulting in an increase in the exergy loss of the system and a decrease in the exergy efficiency. The highest amount of system efficiency belongs to system 2, as well as the least to system 1.

On one hand, the energy efficiency and the exergy efficiency calculated in the solar dish module of this study are 70 % and 35 – 55 %, respectively. Kasaeian [50] et al. investigated the concentrated solar dish system considering the same heat loss as this work and the same work fluids. They concluded that the energy efficiency is around 70 % and the exergy efficiency is above 30 % in the solar dish system. On the other hand, Table 3 shows the distribution of the products in this work which is within the

609 range of direct radiation gasification at the same temperature studied by Kodama [51]
610 et. al and the range of indirect radiation gasification studied by Li [52] et. al. Meanwhile,
611 the system energy efficiency is improved from 37.2 % in the Ref. [52].

612 6 Conclusion

613 In summary, this work designed a novel experimental solar radiation gasification
614 thermogravimetric device. Furthermore, this work set up a solar gasification system
615 energy and exergy analysis model. With the technological analysis of thermodynamics,
616 energy, and exergy, this work investigated the performances of different radiation forms
617 on solar catalytic gasification. Besides that, this work studied the energy and exergy
618 efficiency of the solar, gasifier module, and the system, respectively. With thermal from
619 solar energy, coal and CO_2 are used as reactants, and the products are used in the
620 chemical industry. This chemical process is an important industrial approach to the low-
621 carbon use of coal resources. Limited by the experimental conditions, the economic
622 analysis of different CO_2 mass flow radiation catalytic gasification will be investigated
623 in the future to meet industrial production. The specific main results are as follows:

624 (1) Direct radiation gasification can improve the average carbon conversion rate. This
625 work compares two radiation forms: direct and indirect radiation gasification. It was
626 found that the carbon conversion rate of direct radiation was 15.2 % higher than that of
627 indirect radiation gasification. Meanwhile, the energy conversion efficiency was
628 increased by 3.73 %.

629 (2) The reaction degree is more intense with high gas production rate under direct
630 radiation gasification. From the kinetic analysis, the TG curve of direct radiation

gasification decreases more rapidly at the same temperature, and the DTG curve shifts upward by 34%.

(3) Only adding catalysts cannot solve the low efficiency of indirect radiation gasification at this experimental condition. Catalyst addition can only increase the weight loss rate of indirect radiation from 8 % to 13.2 %, but that of direct radiation is 34.65 %. The addition of catalyst and direct radiation can significantly improve the efficiency of coal gasification. In direct catalytic radiation gasification, the weight loss reaches up to 90 % with the synergistic effect of light and heat (the remaining is ash).

(4) Meanwhile, this work investigates the catalyst ratios in kinetics under direct catalytic radiation gasification. It was found that the 10% ratio is more suitable for system analysis. Direct catalytic radiation at a lower gasification temperature (800 °C) can improve the carbon conversion to 99 %, the energy upgrading factor to 0.86, and the energy conversion efficiency to 11 %.

(5) In dish-type concentrated solar systems, solar and catalyst synergistic effects can increase system efficiency up to 41%. Compared to indirect radiation, direct radiation catalytic gasification increases the dish diameter by only 5% but the efficiency by 13%. The gasification conditions are often harsh (high temperature and pressure). But the direct radiation system and catalyst will allow solar coal thermochemical conversion to be available.

(6) Solar irradiation and ambient temperature can affect the solar dish exergy. Meanwhile, the catalysis addition and the direct radiation form can improve the value of the exergy efficiency of solar coal gasification. The solar dish exergy reaches its peak

in summer (3941.18 W/m^2), and the least value of exergy content belongs in December (1871.57 W/m^2). The highest amount of gasifier exergy efficiency belongs to the direct catalytic radiation gasification (system 3, 29.7 %), as well as the least value of gasifier exergy efficiency implies indirect radiation gasification (system 1, 7.23 %). These results will potentially improve the popularity of new energy sources and the efficiency of resourceful and low-carbon utilization of coal in chemical process.

Acknowledgments

The work is financially supported by the Science and Technology Department of Ningxia Province (No. 2018BCE01004), the National Postdoctoral Program for Innovative Talents of China (BX2021254), China Postdoctoral Science Foundation (2021M702793), and the China Scholarship Council (202106320152).

Appendix A

A.1 Reactor

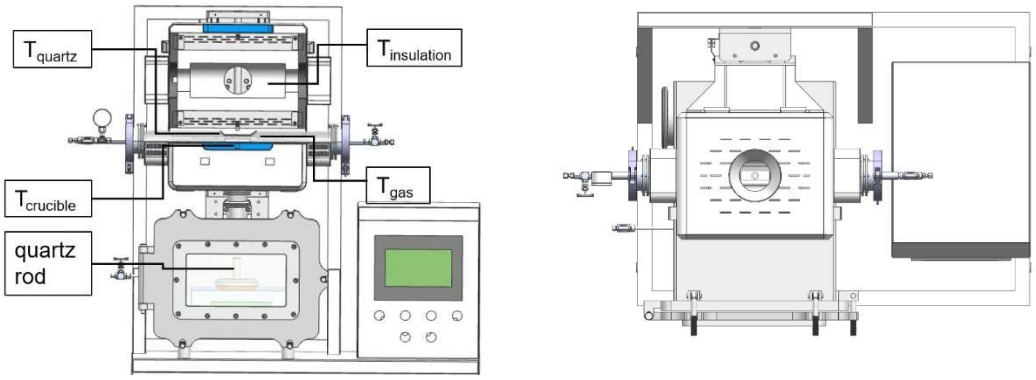

(a) Main view (b) Top view

Figure A1 Reactor

The reactor in the radiation gasification-thermogravimetric test bench based on full-

spectrum concentrated solar energy is shown in Figure A1 (a). Figure A1 (b) shows the top view after the covered insulation. The core reaction zone is made of quartz. The insulation material adopts alumina fiber, which has the characteristics of low thermal conductivity, and thermocouples are arranged in the insulation. The upper part of the insulation is drilled to inject the simulated solar light at a specific angle, and the shell is supported by 5 mm stainless steel (SS304). The T-tube is smoothed in the area irradiated by the simulated sunlight. At the same time, the T-tube is connected to the thermogravimetric chamber. There is an analytical balance with a range of 0-220g and an accuracy of 0.001g in the room. We put a quartz rod to jack up the crucible made of Al_2O_3 to connect the balance and the crucible. N_2 flows into the left side of the thermogravimetric chamber to avoid high-temperature damage to the electronic balance.

A.2 Optical power of simulated solar lights

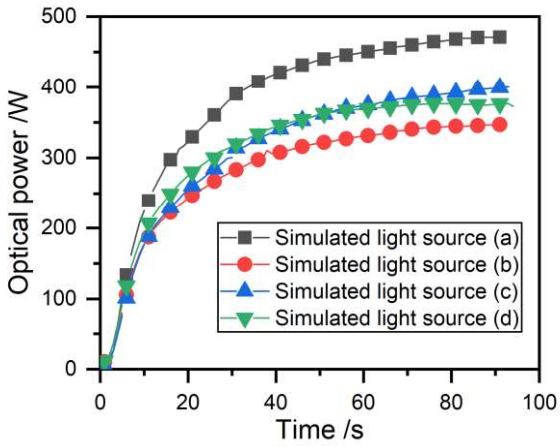

Figure A2 Time evolution of simulated lights' power

The spot power of the xenon lamp irradiated to the crucible was measured using an optical power detection device, HP100A-4KW-HE, provided by Gentec, and Figure A2 shows the measurement results. After 80 s of irradiation, all four simulated lights (a, b,

c and d) reached a steady state. The radiation power delivered to the radiation gasifier needs to be adjusted in a typical radiation gasification experiment. The heat stages include preheating, rated heating, and steady-state heating in sequence. The calculation gives a total simulated solar radiation input power of 1594.44 W

Appendix B

Appendix B introduces the calculation process of the energy analysis model and the monthly evolution solar irradiation model of solar concentrating radiation gasification.

B.1 Energy analysis model

Assume that the average input of the sun to the dish concentrator is 1000W/m^2 [7]:

$$G = 1000\ W/m^2 \tag{B1}$$

The focal length (f) and condensing ratio (C) are calculated as follows [53]:

$$f = \frac{d_d}{4\tan(\psi_{rim/2})} \tag{B2}$$

$$\mathrm{C} = (\frac{d_d}{d_{ap}})^2 \tag{B3}$$

where d_d is the diameter of the dish, d_{ap} is the diameter of the aperture, ψ_{rim} is the rim angle.

Dish solar concentrators use a dual-axis tracking mechanism that continuously tracks the sun to collect maximum sunlight, so the angle of incidence is always equal to zero.

Table B1 The technical specifications of solar collector

System	f	C	Operating type
System 1	0.47	243.36	Dual-Axis mode
System 2	0.42	196.00	Dual-Axis mode

System 3	0.49	268.96	Dual-Axis mode

In our model, the collection and gasifier are integrated, so that the collection temperature is the same as the gasification temperature (1073 K), which is determined. Meanwhile, the concentration ratios used were 243.36, 196.00, and 268.96, respectively. With the same collection temperature and similar concentration, the energy efficiency can be compared to show the catalyst performance. The collection efficiency of systems is 62.2 %, 55.49%, and 64.85 %, respectively. The effect of concentration ratio is included in the system efficiency as a dependent variable, not an independent variable.

Convective heat transfer coefficient through the receiver cavity, Nussle number natural convective heat transfer coefficient, forced convective heat transfer coefficient, and total convective heat transfer coefficient are expressed as [54]:

$$\mathrm{Nu}_{natural} = 0.088 \cdot Gr^{1/3} \cdot \left(\frac{T_{cav}}{T_{amb}}\right)^{0.18} \cdot (cos\theta)^{2.47} \cdot \left(\frac{d_{ap}}{d_{cav}}\right)^{-0.982 \cdot \left(\frac{d_{ap}}{d_{cav}}\right) + 1.12} \quad \text{(B4)}$$

$$\mathrm{h}_{forced} = 0.1967 \cdot v^{1.849} \quad \text{(B5)}$$

$$\mathrm{h}_{total} = \mathrm{h}_{natural} + \mathrm{h}_{forced} \quad \text{(B6)}$$

where Gr is Grashov number, T_{cav} is the temperature of the receiver cavity, T_{amb} is the temperature of ambient, θ is the incident angle, v is the wind speed (m/s).

Reflected and emitted radiative heat transfer from the receiver cavity:

$$\dot{\mathrm{Q}}_{reflected} = (1 - \alpha_{eff}) \cdot \eta_{conc} \cdot G \cdot \mathrm{A}_d \quad \text{(B7)}$$

$$\dot{\mathrm{Q}}_{emitted} = \varepsilon \cdot A_{ap} \cdot \sigma(T_{cav}^4 - T_{amb}^4) \quad \text{(B8)}$$

Where

$$\alpha_{eff} = \alpha_{eff}/[\alpha_{cav} + (1 - \alpha_{cav})/(A_{ap}/\mathrm{A}_{cav})] \quad \text{(B9)}$$

α is the absorptivity, A is the area, and η_{conc} is the efficiency of the concentrator.

The conduction, convection, radiation, and total heat losses of the receiver are expressed as:

$$\dot{Q}_{conduction} = \frac{T_{cav} - T_{amb}}{\ln\left[\frac{\frac{d_{cav}}{2} + \delta_{insul}}{\frac{d_{cav}}{2}}\right] / (2\pi k_{insul} L_{cav})} \quad \text{(B10)}$$

$$\dot{Q}_{convection} = h_{total} \cdot A_{cav} \cdot (T_{cav} - T_{amb}) \quad \text{(B11)}$$

$$\dot{Q}_{radiation} = \dot{Q}_{reflected} + \dot{Q}_{emitted} \quad \text{(B12)}$$

$$\dot{Q}_{L,dish} = \dot{Q}_{conduction} + \dot{Q}_{convection} + \dot{Q}_{radiation} \quad \text{(B13)}$$

where δ_{insul} is the thickness of insulation.

The efficiency of the receiver is calculated as

$$\eta_{rec} = 1 - \frac{\dot{Q}_{total}}{\eta_{conc} \cdot G \cdot A_d} \quad \text{(B14)}$$

The energy input to the coal gasification reactor is

$$\dot{Q}_{input} = \eta_{rec} \cdot \eta_{conc} \cdot G \cdot A_d \quad \text{(B15)}$$

The heat loss through the wall is about 1.7% of the heat value of coal input [29]:

$$\dot{Q}_{wall} = 17\ W \quad \text{(B16)}$$

Sensible heat loss in output gas [46]：

$$\dot{Q}_{sensible} = (\dot{m}_{CO} \cdot c_{CO} + \dot{m}_{CO_2,out} \cdot c_{CO_2} + \dot{m}_{CH_4} \cdot c_{CH_4} + \dot{m}_{H_2} \cdot c_{H_2} + \dot{m}_{N_2} \cdot c_{N_2}) \cdot T_{output} \quad \text{(B17)}$$

$$\dot{Q}_{pg} = \dot{m}_p LHV_p \quad \text{(B18)}$$

where T_{output} is the temperature of the reactor export, $\dot{m}$ is the mass flow, and c is the specific heat capacity.

The specific heat capacity is expressed as:

$$C_{p_i} = a + bT + cT^2 + dT^3 \quad \text{(B19)}$$

where a, b, c, and d are the specific gas product specific heat capacity coefficient[55].

B.2 The monthly evolution solar irradiation model

The solar irradiation outside the earth (G_{on}) is expressed according to eq. (B20) [56]：

$$G_{on} = G_{SC}(1.000110 + 0.034221cosB + 0.001280sinB + 0.000719cos2B +$$

$$0.000077sin2B) \quad \text{(B20)}$$

where G_{SC} is the solar constant ($1367\ W/m^2$), $B = (n-1) \times 360/365$, n is the n-th of one year.

The declination angle (δ) is expressed according to eq. (B21) :

$$\delta = (\frac{180}{\pi})(0.006918 - 0.399912cosB + 0.070257sinB - 0.006758cos2B + 0.000907sin2B - 0.002697cos3B + 0.00148sin3B) \quad \text{(B21)}$$

The zenith angle (θ_z) is expressed according to eq. (B22):

$$cos\theta_z = cos\varphi cos\delta cos\omega + sin\varphi sin\delta \quad \text{(B22)}$$

where φ is the latitude (°), and ω is the time angle (°).

The atmospheric transmittance (τ_b) is expressed according to eq. (B23):

$$\tau_b = a_0 + a_1 \exp\left(-\frac{k}{cos\theta_z}\right) \quad \text{(B23)}$$

where a_0, a_1 are the constant of the atmospheric transmittance formula, and k is thermal conductivity ($W/(m \cdot K)$)

Solar irradiation (I_b) on inclined surfaces can be expressed according to eq. (B24):

$$I_b = G_{on}\tau_b cos\theta \quad \text{(B24)}$$

where θ is the incidence angle (°).

Dish solar concentrators use a dual-axis tracking mechanism that continuously tracks the sun to collect maximum sunlight, so the angle of incidence is always equal to zero ($cos\theta = 1$).

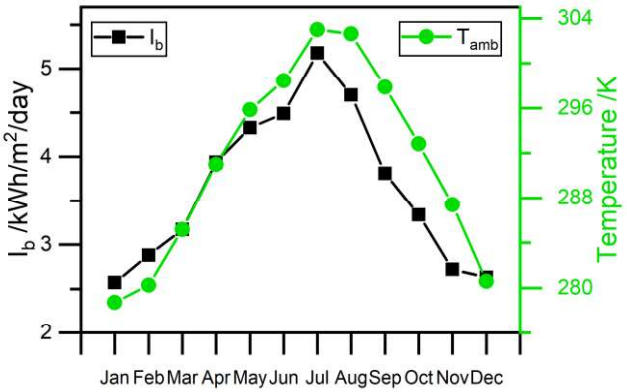

773

774 Figure B1 The monthly evolution of I_b and T_{amb}.

775 With this calculation process, Figure B1 shows the monthly evolution of solar

776 irradiation. Meanwhile, we obtain the monthly evolution of ambient temperature in

777 Hangzhou on the website [48].

778

References

[1] T. Wilberforce, A.G. Olabi, E.T. Sayed, K. Elsaid, M.A. Abdelkareem, Progress in carbon capture technologies, Sci. Total Environ. 761 (2021) 143203. https://doi.org/10.1016/j.scitotenv.2020.143203.

[2] X. Zhao, X. Ma, B. Chen, Y. Shang, M. Song, Challenges toward carbon neutrality in China: Strategies and countermeasures, Resour. Conserv. Recycl. 176 (2022) 105959. https://doi.org/10.1016/j.resconrec.2021.105959.

[3] Z. Zhou, L. Guo, L. Chen, S. Shan, Z. Wang, Study of pyrolysis of brown coal and gasification of coal-water slurry using the ReaxFF reactive force field, Int. J. Energy Res. 42 (2018) 2465–2480. https://doi.org/10.1002/er.4029.

[4] D. Yadav, R. Banerjee, A review of solar thermochemical processes, Renew. Sustain. Energy Rev. 54 (2016) 497–532. https://doi.org/10.1016/j.rser.2015.10.026.

[5] J.W.K. Norman C. Ford, Solar Power, Bull. At. Sci. 3402 (1971) 1–27. https://doi.org/10.1080/00963402.1971.11455398.

[6] S. Abanades, P. Charvin, G. Flamant, P. Neveu, Screening of water-splitting thermochemical cycles potentially attractive for hydrogen production by concentrated solar energy, Energy. 31 (2006) 2805–2822. https://doi.org/10.1016/j.energy.2005.11.002.

[7] A. Steinfeld, Solar thermochemical production of hydrogen - A review, Sol. Energy. 78 (2005) 603–615. https://doi.org/10.1016/j.solener.2003.12.012.

[8] A. Kogan, Direct solar thermal splitting of water and on-site separation of the products - IV. Development of porous ceramic membranes for a solar thermal water-splitting reactor, Int. J. Hydrogen Energy. 25 (2000) 1043–1050. https://doi.org/10.1016/S0360-3199(00)00024-0.

[9] C.J. Yang, R.B. Jackson, China's growing methanol economy and its implications for energy and the environment, Energy Policy. 41 (2012) 878–884. https://doi.org/10.1016/j.enpol.2011.11.037.

[10] I. Janajreh, I. Adeyemi, S.S. Raza, C. Ghenai, A review of recent developments and future prospects in gasification systems and their modeling, Renew. Sustain. Energy Rev. 138 (2021) 110505. https://doi.org/10.1016/j.rser.2020.110505.

[11] P. v. Zedtwitz, A. Steinfeld, The solar thermal gasification of coal - Energy conversion efficiency and CO2 mitigation potential, Energy. 28 (2003) 441–456. https://doi.org/10.1016/S0360-5442(02)00139-1.

[12] D.W. Gregg, R.W. Taylor, J.H. Campbell, J.R. Taylor, A. Cotton, Solar gasification of coal, activated carbon, coke and coal and biomass mixtures, Sol. Energy. 25 (1980) 353–364. https://doi.org/10.1016/0038-092X(80)90347-3.

[13] T. Kodama, N. Gokon, S.I. Enomoto, S. Itoh, T. Hatamachi, Coal coke gasification in a windowed solar chemical reactor for beam-down optics, J. Sol. Energy Eng. Trans. ASME. 132 (2010) 1–6. https://doi.org/10.1115/1.4002081.

[14] A. Z'Graggen, P. Haueter, D. Trommer, M. Romero, J.C. de Jesus, A. Steinfeld, Hydrogen production by steam-gasification of petroleum coke using concentrated solar power-II Reactor design, testing, and modeling, Int. J. Hydrogen Energy. 31 (2006) 797–811. https://doi.org/10.1016/j.ijhydene.2005.06.011.

[15] H. Weldekidan, V. Strezov, G. Town, Review of solar energy for biofuel extraction, Renew. Sustain. Energy Rev. 88 (2018) 184–192. https://doi.org/10.1016/j.rser.2018.02.027.

[16] H. Wu, Q. Liu, Z. Bai, G. Xie, J. Zheng, B. Su, Thermodynamics analysis of a novel steam/air biomass gasification combined cooling, heating and power system with solar energy, Appl. Therm. Eng. 164 (2020) 114494. https://doi.org/10.1016/j.applthermaleng.2019.114494.

[17] N. Gokon, S. Kumaki, Y. Miyaguchi, S. Bellan, T. Kodama, H. Cho, Development of a 5kWth internally circulating fluidized bed reactor containing quartz sand for continuously-fed coal-coke gasification and a beam-down solar concentrating system, Energy. 166 (2019) 1–16. https://doi.org/10.1016/j.energy.2018.10.036.

[18] Q. Bellouard, S. Rodat, S. Abanades, S. Ravel, P.É. Frayssines, Design, simulation and experimental study of a directly-irradiated solar chemical reactor for hydrogen and syngas production from continuous solar-driven wood biomass gasification, Int. J. Hydrogen Energy. 4 (2019) 19193–19205. https://doi.org/10.1016/j.ijhydene.2018.04.147.

[19] F. Müller, H. Patel, D. Blumenthal, P. Poživil, P. Das, C. Wieckert, P. Maiti, S. Maiti, A. Steinfeld, Co-production of syngas and potassium-based fertilizer by solar-driven

thermochemical conversion of crop residues, Fuel Process. Technol. 171 (2018) 89–99. https://doi.org/10.1016/j.fuproc.2017.08.006.
[20] N. Piatkowski, C. Wieckert, A.W. Weimer, A. Steinfeld, Solar-driven gasification of carbonaceous feedstock - A review, Energy Environ. Sci. 4 (2011) 73–82. https://doi.org/10.1039/c0ee00312c.
[21] N. Piatkowski, A. Steinfeld, Solar-driven coal gasification in a thermally irradiated packed-bed reactor, Energy and Fuels. 22 (2008) 2043–2052. https://doi.org/10.1021/ef800027c.
[22] A. Muroyama, T. Shinn, R. Fales, P.G. Loutzenhiser, Modeling of a Dynamically-Controlled Hybrid Solar/Autothermal Steam Gasi fi cation Reactor, (2014).
[23] N. Gokon, R. Ono, T. Hatamachi, L. Liuyun, H.J. Kim, T. Kodama, CO2 gasification of coal cokes using internally circulating fluidized bed reactor by concentrated Xe-light irradiation for solar gasification, Int. J. Hydrogen Energy. 37 (2012) 12128–12137. https://doi.org/10.1016/j.ijhydene.2012.05.133.
[24] T. Kodama, Y. Kondoh, T. Tamagawa, A. Funatoh, K.-I. Shimizu, Y. Kitayama, Fluidized Bed Coal Gasification with CO 2 under Direct Irradiation with Concentrated Visible Light, Energy & Fuels. 16 (2002) 1264–1270. https://doi.org/10.1021/ef020053x.
[25] M. Mehrpooya, M. Dehqani, S.A. Mousavi, S.A. Moosavian, Heat transfer and economic analyses of using various nanofluids in shell and tube heat exchangers for the cogeneration and solar-driven organic Rankine cycle systems, Int. J. Low-Carbon Technol. 17 (2022) 11–22. https://doi.org/10.1093/ijlct/ctab075.
[26] S.A. Mousavi, M. Mehrpooya, M.A.V. Rad, M.H. Jahangir, A new decision-making process by integration of exergy analysis and techno-economic optimization tool for the evaluation of hybrid renewable systems, Sustain. Energy Technol. Assessments. 45 (2021) 101196. https://doi.org/10.1016/j.seta.2021.101196.
[27] S.A. Mousavi, M. Mehrpooya, M. Delpisheh, Development and life cycle assessment of a novel solar-based cogeneration configuration comprised of diffusion-absorption refrigeration and organic Rankine cycle in remote areas, Process Saf. Environ. Prot. 159 (2022) 1019–1038. https://doi.org/10.1016/j.psep.2022.01.067.
[28] X. Cai, S. Shan, Q. Zhang, J. Zhao, Z. Zhou, New WSGG model for gas mixtures of H2O, CO2, and CO in typical coal gasifier conditions, Fuel. 311 (2022) 122541. https://doi.org/10.1016/j.fuel.2021.122541.
[29] E. Terrell, C.S. Theegala, Thermodynamic simulation of syngas production through combined biomass gasification and methane reformation, Sustain. Energy Fuels. 3 (2019) 1562–1572. https://doi.org/10.1039/C8SE00638E.
[30] Y. Bai, P. Lv, F. Li, X. Song, W. Su, G. Yu, Investigation into Ca/Na compounds catalyzed coal pyrolysis and char gasification with steam, Energy Convers. Manag. 184 (2019) 172–179. https://doi.org/10.1016/j.enconman.2019.01.063.
[31] J. Kopyscinski, R. Habibi, C.A. Mims, J.M. Hill, K2CO3-Catalyzed CO2 Gasification of Ash-Free Coal: Kinetic Study, Energy & Fuels. 27 (2013) 4875–4883.
[32] J. Kopyscinski, M. Rahman, R. Gupta, C.A. Mims, J.M. Hill, K2CO3 catalyzed CO2 gasification of ash-free coal. Interactions of the catalyst with carbon in N2 and CO2 atmosphere, Fuel. 117 (2014) 1181–1189. https://doi.org/10.1016/j.fuel.2013.07.030.
[33] S. Islam, J. Kopyscinski, S.C. Liew, J.M. Hill, Impact of K2CO3 catalyst loading on the CO2-gasification of Genesse raw coal and low-ash product, Powder Technol. 290 (2016) 141–147. https://doi.org/10.1016/j.powtec.2015.12.013.
[34] X. Zhou, W. Li, R. Mabon, L.J. Broadbelt, A mechanistic model of fast pyrolysis of hemicellulose, Energy Environ. Sci. 11 (2018) 1240–1260. https://doi.org/10.1039/c7ee03208k.
[35] K.J. Laidler, The development of the arrhenius equation, J. Chem. Educ. 61 (1984) 494–498. https://doi.org/10.1021/ed061p494.
[36] J.C.G. da Silva, J.L.F. Alves, W.V. de A. Galdino, S.L.F. Andersen, R.F. de Sena, Pyrolysis kinetic evaluation by single-step for waste wood from reforestation, Waste Manag. 72 (2018) 265–273. https://doi.org/10.1016/j.wasman.2017.11.034.
[37] S.R. Naqvi, R. Tariq, Z. Hameed, I. Ali, M. Naqvi, W.H. Chen, S. Ceylan, H. Rashid, J. Ahmad, S.A. Taqvi, M. Shahbaz, Pyrolysis of high ash sewage sludge: Kinetics and thermodynamic analysis using Coats-Redfern method, Renew. Energy. 131 (2019) 854–860. https://doi.org/10.1016/j.renene.2018.07.094.
[38] P. Li, Q. Yu, Q. Qin, W. Lei, Kinetics of CO2/coal gasification in molten blast furnace slag,

Ind. Eng. Chem. Res. 51 (2012) 15872–15883. https://doi.org/10.1021/ie301678s.
[39] S. Shan, Z. Zhou, Z. Wang, K. Cen, A novel flame energy grading conversion system: Preliminary experiment and thermodynamic parametric analysis, Int. J. Energy Res. 44 (2020) 2084–2099. https://doi.org/10.1002/er.5066.
[40] A.S. Joshi, I. Dincer, B. V. Reddy, Performance analysis of photovoltaic systems: A review, Renew. Sustain. Energy Rev. 13 (2009) 1884–1897. https://doi.org/10.1016/j.rser.2009.01.009.
[41] C. Michalakakis, A.G. Hernandez, J. Fouillou, J.M. Cullen, R.C. Lupton, Calculating the chemical exergy of materials, J. Ind. Ecol. (2021) 274–287. https://doi.org/10.1111/jiec.13120.
[42] M. Gräbner, B. Meyer, Performance and exergy analysis of the current developments in coal gasification technology, Fuel. 116 (2014) 910–920. https://doi.org/10.1016/j.fuel.2013.02.045.
[43] J.M. Sanchez-Hervas, G.M. Moya, I. Ortiz-González, Current status of coal gasification, New Trends Coal Convers. Combust. Gasification, Emiss. Coking. (2018) 175–202. https://doi.org/10.1016/B978-0-08-102201-6.00007-8.
[44] Z. Zhou, Q. Zhang, L. Chen, Experimental Analysis of Intrinsic Kinetics and Rate Profiles for Coal Char Conversion under Different Atmospheres, Combust. Sci. Technol. 00 (2021) 1–18. https://doi.org/10.1080/00102202.2021.1973448.
[45] A. Sharma, T. Takanohashi, I. Saito, Effect of catalyst addition on gasification reactivity of HyperCoal and coal with steam at 775-700 °C, Fuel. 87 (2008) 2686–2690. https://doi.org/10.1016/j.fuel.2008.03.010.
[46] L. Xu, J. Yuan, Thermodynamic properties calculation of the flue gas based on its composition estimation for coal-fired power plants, Appl. Therm. Eng. 90 (2015) 366–375. https://doi.org/10.1016/j.applthermaleng.2015.07.018.
[47] N. Fang, L. Zeng, B. Zhang, Z. Li, H. Wang, X. Liu, Numerical simulation of flow and gasification characteristics with different swirl vane angles in a 2000 t/d GSP gasifier, Appl. Therm. Eng. 153 (2019) 791–799. https://doi.org/10.1016/j.applthermaleng.2019.03.006.
[48] C.M. Administration, https://en.wikipedia.org/wiki/Hangzhou, (n.d.).
[49] S. Sukumaran, K. Sudhakar, Performance analysis of solar powered airport based on energy and exergy analysis, Energy. 149 (2018) 1000–1009. https://doi.org/10.1016/j.energy.2018.02.095.
[50] A. Kasaeian, A. Kouravand, M.A. Vaziri Rad, S. Maniee, F. Pourfayaz, Cavity receivers in solar dish collectors: A geometric overview, Renew. Energy. 169 (2021) 53–79. https://doi.org/10.1016/j.renene.2020.12.106.
[51] T. Kodama, Y. Kondoh, T. Tamagawa, A. Funatoh, K.I. Shimizu, Y. Kitayama, Fluidized bed coal gasification with CO2 under direct irradiation with concentrated visible light, Energy and Fuels. 16 (2002) 1264–1270. https://doi.org/10.1021/ef020053x.
[52] X. Li, J. Chen, Q. Hu, P. Chu, Y. Dai, C.-H. Wang, Solar-driven gasification in an indirectly-irradiated thermochemical reactor with a clapboard-type internally-circulating fluidized bed, Energy Convers. Manag. 248 (2021) 114795. https://doi.org/10.1016/j.enconman.2021.114795.
[53] W.B. Stine, R.B. Diver, A compendium of solar dish/Stirling technology, SAND93-7026 UC-236, (1994). http://www.osti.gov/energycitations/servlets/purl/10130410-xiVU1V/native/%5Cn10.2172/10130410.
[54] S.Y. Wu, L. Xiao, Y. Cao, Y.R. Li, Convection heat loss from cavity receiver in parabolic dish solar thermal power system: A review, Sol. Energy. 84 (2010) 1342–1355. https://doi.org/10.1016/j.solener.2010.04.008.
[55] R. Lanzafame, M. Messina, A new method for the calculation of gases enthalpy, in: 35th Intersoc. Energy Convers. Eng. Conf. Exhib., 2000: pp. 318–328.
[56] M. Boxwell, Solar electricity handbook: A simple, practical guide to solar energy-designing and installing photovoltaic solar electric systems, Greenstream publishing, 2010.

Coal gasification process driven by concentrated solar radiation for carbon neutralization: reaction and energy characteristics

Qi Zhang[a,b], Shiquan Shan [a, *], Jinhong Yu [a], Zhijun Zhou [a], Kai H. Luo [b]

[a] *State Key Laboratory of Clean Energy Utilization, Zhejiang University, Hangzhou 310027, Zhejiang, P.R. China;* [b.] *Department of Mechanical Engineering, University College London, Torrington Place, London WC1E 7JE, UK*

*Corresponding author e-mail: shiquan1204@zju.edu.cn

Abstract

Solar-driven gasification products for chemical feedstock are one of the effective means to utilize coal in a low-carbon and resourceful way. However, few studies on the reaction and energy characteristics are based on experimental data of concentrated solar coal gasification. This study designed a novel experimental solar radiation gasification thermogravimetric device. An energy model of a solar radiation dish thermochemical conversion system was also developed. Compared to indirect radiation, direct radiation has a 10 % higher carbon conversion rate, an increased energy upgrade factor (up to 0.86), and a 38.5 % increase in energy conversion efficiency. Furthermore, we investigate direct radiation-catalyzed gasification to assess the effects of different types and ratios of catalysts. The results showed that the catalytic effect of K_2CO_3 was better than that of Na_2CO_3, which would improve the energy conversion efficiency by 4.8 %. For K_2CO_3, the efficiency was increased by 14.1 % through increasing the doping ratio from 5 % to 10 %. Meanwhile, this study analyzed the reaction kinetics of direct radiation-catalyzed gasification. Finally, we constructed a solar concentrating radiation dish thermochemical conversion system model based on the experimental data. We

found that the system energy efficiency in the direct radiation form was 15.3 % higher than that in the indirect radiation form; besides, adding the catalyst in the direct radiation form increased the energy efficiency by 23.8 %. We also found that the gasifier exergy efficiency in direct radiation catalyst gasification was 29.7 %, and that of indirect radiation gasification was 7.23 %. The monthly solar exergy distribution follows the solar radiation closely. The results guide the chemical process of solar thermal conversion.

Keywords: solar energy; radiation gasification; thermochemical conversion; catalytic; kinetics

1 Introduction

Coal has massive reserves, and its use as a fuel for a long time has resulted in significant carbon emissions. In recent years, many countries have announced carbon-neutral energy policies. It is necessary to capture carbon in the energy production process [1] and develop renewable energy [2]. Therefore, the proportion of coal used as a fuel is gradually decreasing. But low-carbon emission utilization of coal is an essential research theme in the face of its huge reserves. Coal gasification is a vital means of clean and efficient utilization [3]. It can generate syngas and is a main feedstock for the chemical industry. The traditional process uses the heat from combustion to power the gasification, which does not meet carbon-neutral requirements. Therefore, renewable energy sources such as solar energy are required to drive the coal gasification process.

Solar energy is the primary sustainable energy source. The solar-driven coal gasification is based on a solar thermochemical energy conversion process. Researchers initiated thermochemical studies of water for hydrogen production due to the petroleum crisis [4], which also marks the beginning of the investigation into solar thermochemical conversion. During the solar thermochemical hydrogen production process, solar energy is concentrated to generate high temperatures so that water is split into hydrogen and oxygen [5]. However, this process requires a temperature as high as 2300 °C [6] and exceptional devices to separate hydrogen and oxygen from the mixture [7]. With the development of solar-concentrating technology and membrane technology, Abraham Kogan [8] proposed a porous ceramic membrane reactor, which added a

catalyst to water so that the water-splitting process could be carried out in multiple steps. Hydrogen and oxygen are generated in different reactions, avoiding the separation. At the same time, this process will lower the reaction temperature to below 1500°C. This process is the thermochemical cycle hydrogen production method. However, this method still has problems such as high reaction equilibrium temperature, which leads to increased heat conduction and heat radiation losses; and poor oxygen carrier kinetics, which leads to a long reaction cycle time. Consequently, researchers introduced carbon cycling, such as methanol steam reforming, to significantly reduce the reaction temperature. Yang [9] et al. reviewed the current methanol policy. The current methanol production route relies heavily on coal, ultimately increasing net greenhouse gas emissions and exacerbating coal market volatility, inconsistent with the carbon neutrality goals. With the widespread and large reserves of fossil raw materials, coal pyrolysis and gasification driven by solar energy have also attracted the attention of researchers. This chemical process is more mature than methane steam reforming and can realize the storage of solar energy and reduce CO_2 emission. Meanwhile, coal as a gasification feedstock has a syngas capacity of about 330 GWth, representing 76.7 % of all gasification feedstocks in the industry [10]. Thus, it has an irreplaceable role in producing fuels and chemical raw materials acting as a bridge for the transition from conventional to clean energy sources.

Solar concentrating technologies can generate a high temperature, which is especially suitable for coal gasification [11]. Researchers have investigated the solar coal gasification process on raw materials, reactors, and energy utilization forms. Gregg

et al. [12] studied solar coal gasification, using bituminous coal, activated carbon, coke, coal and biomass as raw materials, and estimated that about 60% of the solar energy entering the reactor was stored. Kodama et al. [13] conducted a high flux visible light coal gasification experiment in a small quartz reactor. They found that the fraction of incident light energy stored by CO is about 8%. Graggen [14] et al. designed an entrained-flow gasification reactor for gasification with a continuous stream vortex, resulting in an energy conversion efficiency of 9%. Weldekidan [15] et al. investigated different forms of concentrating technology in solar thermal conversion and believed that the parabolic disk form has the highest solar energy capture rate, with an optical efficiency of 94%. Wu [16] et al. proposed a dish system to collect solar energy to generate high-temperature steam, which acts as an agent to drive gasification. The primary energy efficiency reaches 51.34%. Generally, existing solar-driven coal gasification radiation forms mainly include direct radiation [17,18] and indirect radiation [19–21]. Direct radiation means that solar radiation directly enters the reactor through the quartz window and drives the gasification chemical process. Indirect radiation means that the solar is concentrated to heat the absorber and coal gasification is driven by thermal energy. Then the heat is transferred to the coal gasification reaction. Haftom [15] et al. analyzed these two energy utilization forms of carbon-based fuels. The study showed that the indirect radiation form can overcome the challenge of keeping the window clean. However, the heat transfer efficiency is lower than that of the direct radiation form. The concept of direct radiation bypasses the limitations imposed by conduction heat transfer through the ceramic walls, thus ensuring high

energy conversion efficiency. The main indicators of solar coal gasification performance: energy upgrade factor [20], that is, the ratio of the heat value of syngas to the heat value of raw materials, and energy conversion efficiency [22], that is, the ratio of the heat value of syngas and the sum of the heat value of solar energy and raw materials. Gokon [23] et al. investigated the coke gasification kinetic based on either the homogeneous or the shrinking core kinetic model and concluded that the form of circulation has a great influence on the conversion rate of gasification with the fluidized bed. Kodama [24] et al. studied the effects of metal oxides as filler materials on the kinetics of fluidized beds driven by solar energy. However, there is a lack of online thermogravimetric experimental data and a lack of kinetic and energy analysis of solar catalytic gasification. Mehrpooya [25] et al. studied the economics of solar-driven tube heat transfer and concluded that the use of nanofluids can significantly reduce the cost. Mousavi conducted the exergy analysis of the solar system. They obtained the trends in economics of exergy to months [26]and evaluated the life cycle of solar concentrating systems in remote areas[27]. Although exergy analysis of solar-driven power utilization systems has been studied, existing solar coal gasification research lacks kinetic and chemical process energy analysis based on experimental data. Thus, it is difficult to provide some guiding suggestions for actual industrial production. Meanwhile, there are few exergy analysis investigations on solar catalytic gasification systems with different solar irradiation.

In the industrial production of coal gasification, a high-temperature and high-pressure environment is required to achieve high conversion efficiency [28]. However,

125 it is difficult to maintain the high temperature and high-pressure gasification state. At
126 the same time, it brings a significant economic burden to the investment and operation
127 of equipment. As a third-generation coal gasification technology, adding a catalyst can
128 reduce the reaction temperature by 200-300 K and achieve mild gasification under
129 normal pressure. Besides, it can also significantly improve the gasification reaction rate
130 and reduce energy consumption as well as equipment and materials requirements. It can
131 directionally adjust the product gas composition, such as the amount of H_2 released
132 [29,30]. It is known by researchers that K_2CO_3 and Na_2CO_3 have a strong catalytic
133 effect on coal gasification. Kopyscinski et al. [31–33] found that K_2CO_3 could reduce
134 the gasification temperature by 240 - 320 °C. The actual production of solar
135 thermochemical conversion is greatly affected by uncontrollable factors. It is
136 challenging to maintain a high-temperature state, and it is challenging to create high-
137 pressure conditions. Therefore, the use of catalysts has a high practical value in the
138 context of solar thermochemical conversion. Catalytic gasification is an important
139 development field of solar coal chemical engineering. However, to the best of the
140 authors' knowledge, there are currently few experimental studies on catalytic coal
141 gasification with online thermodynamics analysis in solar thermochemical conversion.

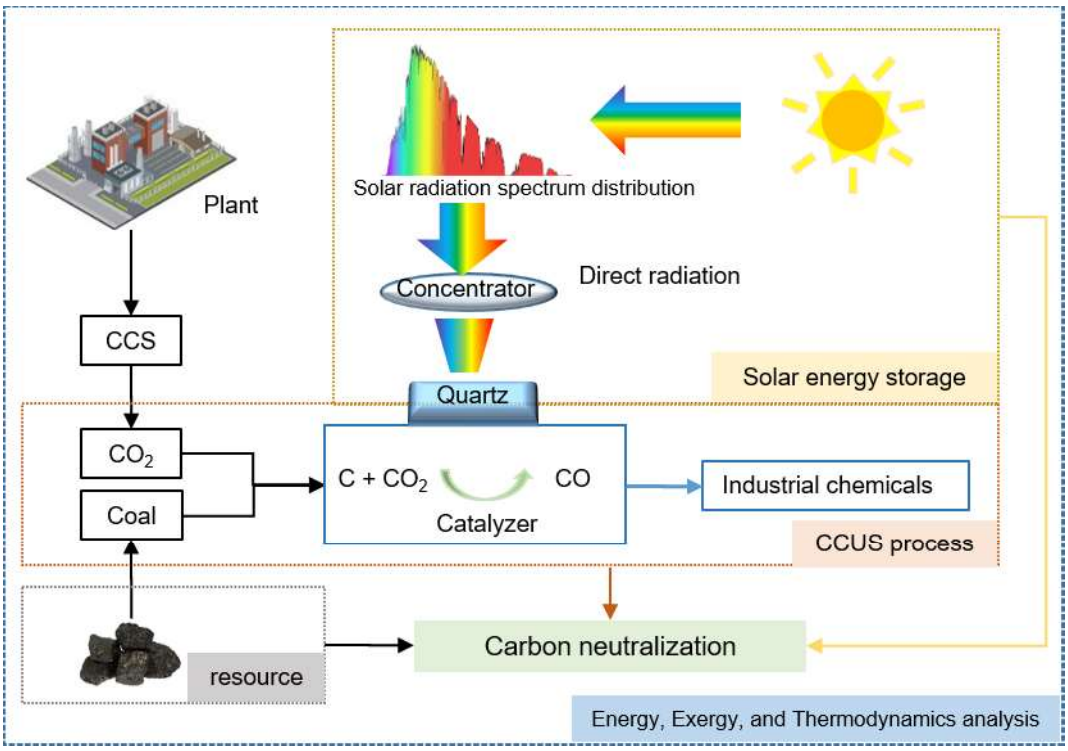

Figure 1 Carbon neutral solar coal gasification technology route

In this paper, a carbon-neutral solar coal gasification technology is proposed. Meanwhile, we independently design and develop a full-spectrum concentrated radiation-driven kinetic analysis test bench for investigating coal gasification reaction characteristics. This technology is based on solar energy to drive the coal gasification process, convert solar energy into fuel chemical energy to achieve solar energy storage, and realize coal resource utilization without combustion. The whole process is a low-carbon process. In addition, solar coal gasification processes using CO_2 captured by carbon capture and storage (CCS) technology as a gasification agent can be regarded as a Carbon Capture, Utilization, and Storage (CCUS) technology. Figure 1 shows that the coal gasification technology route based on concentrated solar-driven is comprehensively in line with the global demand for carbon neutrality. This route has a broad prospect and essential strategic value. Thermodynamic analysis of solar catalytic

gasification is an important part of the chemical process. The novelties of this research are as follows: (1) This work designed a novel experimental solar radiation gasification thermogravimetric device. (2) This work studied the gasification product distribution and the online kinetic analysis of different types and ratios of catalysts on experimental radiation gasification. (3) This work developed the energy and exergy analysis models based on experimental data for the solar gasification chemical process, which provides a reference for the engineering application of solar thermochemical conversion to chemical feedstock.

2 Experiment system and method

2.1 System setup

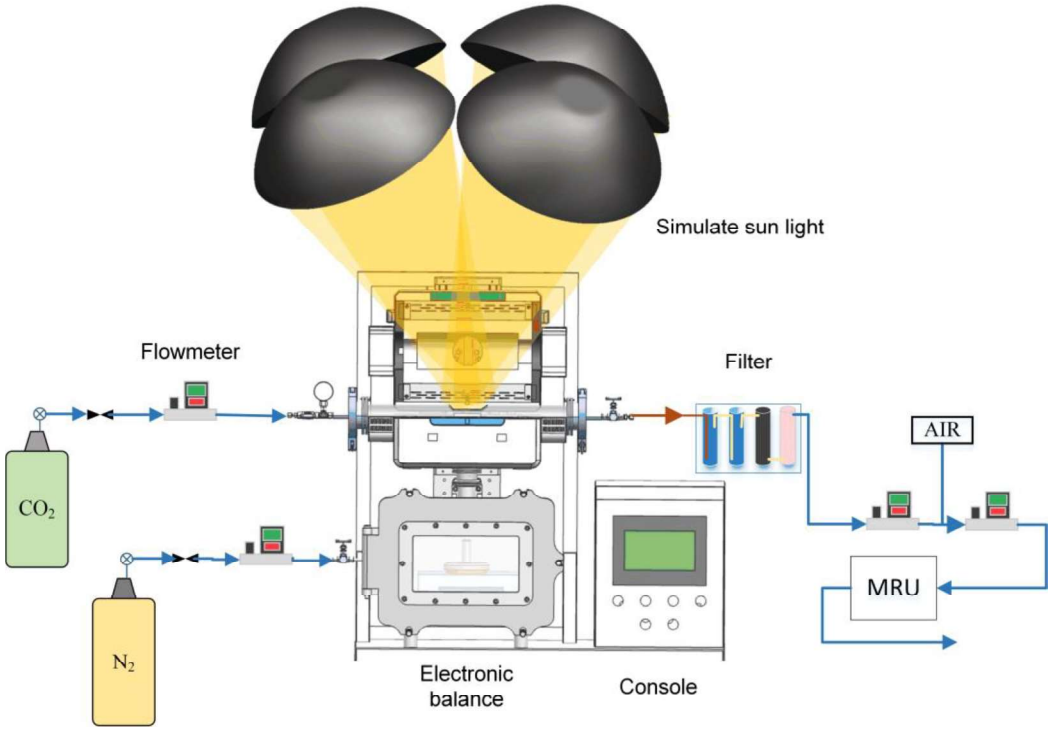

Figure 2 Schematics of the overall experimental setup

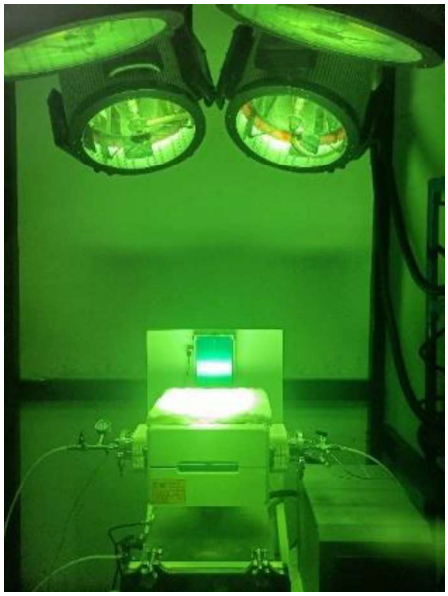

Figure 3 Radiation gasification system (photographed through a black glass sheet)

As shown in Figure 2, we designed and built our experimental setup based on the purpose of coal gasification under the full spectrum of concentrated solar. This setup consists of simulated sunlight, a coal gasification reactor, a thermogravimetric module, and an online flue gas analysis module. First of all, the simulated sunlight comprises four xenon lamps with a single electrical power rating of 0-7 kw, providing the approximate radiation flux of a concentrated solar energy system. The simulated light is adjusted to a spot size of 20 mm to cover the coal powder in the crucible completely. Figure 3 shows the state when running the experiment, where we shoot through the black glass sheet.

Secondly, the coal gasification reactor consists of a T-tube as the main body, which is connected to the thermogravimetric monitoring module underneath and the flue gas analysis module on the right. The coal is contained in a crucible held up by a quartz rod with a thermogravimetric monitoring module connected to the other end of the rod. CO_2 (purity above 99.95%) enters the gasification reactor through the left side of the T-tube.

184 N_2 (purity above 99.99%) enters the gasification reactor through the lower part of the
185 T-tube. It passes through and cools the thermogravimetric monitoring module during
186 the flow. In the reactor, we arranged four Omega type-k thermocouples to monitor the
187 temperature changes of the reaction process online. These locations include the quartz
188 tube irradiation surface, the right part of the T-tube, the crucible, and the insulation,
189 with details in Figure A1 of Appendix A. The gasification products flow to the flue gas
190 analysis module through the right side of the T-tube. Before entering the flue gas
191 analysis instrument (provided by German MRU), the flue gas is cooled and scrubbed
192 twice with pure water, then adsorbed and dried with graphite and SiO_2. Since the gas
193 flow rate is low, a certain amount of air is added in before entering the flue gas analyzer.
194 Finally, the excess gas is released into the vent. Among other things, details of the
195 reactor are in Appendix A.

196 Besides the information above, Hangzhou Jingong Special Company provides the
197 gas cylinder and pressure reducer. Alicat provides the flow meter. The Vario Plus gas
198 analyzer from MRU, Germany, analyzed the product gas components online, which can
199 determine the main components in the product gas, among which H_2 is determined by
200 thermal conductivity doppler (TCD), and the rest components are determined by the
201 non-dispersive infrared principle (NDIR).

202 2.2 Coal

203 The coal type selected for this study is provided by a subsidiary company of
204 Ningxia Coal Group in China. After receiving the coal, we ground, screened, and dried
205 it. The drying was done at 378 K for 12 hours. The coal used in the experiment was all

206 from the same batch.

207 Table 1 Main properties of the used coal

Proximate analysis (wt, ad, %)				Ultimate analysis (wt, ad, %)					$Q_{b,ad}$(MJ/kg)
M	V	FC	A	C	H	O	N	S	
4.15	26.63	59.58	9.64	68.58	3.86	12.40	0.80	0.57	26.66

208 Since there is no oxygen involved in the coal gasification process, the coal will
209 have two stages of endothermic reactions with temperature: pyrolysis and the
210 Boudouard reaction[34],

211 Pyrolysis:

212 $$\mathrm{Coal} \rightarrow \mathrm{C(s)} + \mathrm{CO} + \mathrm{H_2} + \mathrm{CH_4} + \mathrm{CO_2} + \mathrm{tar} + \mathrm{ash} \quad (1)$$

213 The Boudouard reaction：

214 $$\mathrm{C(s)} + \mathrm{CO_2} \rightarrow 2\mathrm{CO},\ \Delta H = 172.4\ \mathrm{kJ/mol} \quad (2)$$

215 2.3 Performance indicators

216 We quantify the radiation gasification performance based on three metrics to analyze
217 the experimental data. The first is the average carbon conversion rate, which is
218 expressed as:

219 $$\bar{X} = \frac{\int \dot{n}_{CO}dt + \int \dot{n}_{CO_2}dt + \int \dot{n}_{CH_4}dt - \int \dot{n}_{CO_{2,in}}dt}{n_{coal}} \quad (3)$$

220 where $\dot{n}_{CH_4}$, $\dot{n}_{CO_2}$, and $\dot{n}_{CO}$ are molar flow rates of CH_4, CO_2, and CO in the output
221 of T-tube, respectively, $\dot{n}_{CO_{2,in}}$ is the CO_2 molar flow rates in the input of T-tube. And
222 n_{coal} is the molar amount of coal fed into the reactor.

223 The second one is the ratio of the lower heating value (LHV) of product gas to the
224 LHV of coal, which is the energy upgrade factor, is expressed as:

$$U = \frac{\int \dot{n}_p LHV_p dt}{m_{coal} LHV_{coal}} \quad (4)$$

where $\dot{n}_p$ is molar flow rates of the product gas, m_{coal} is the mass of coal, LHV_p is the lower heating value of the product gas and the LHV_{coal} is the lower heating value of coal.

Last but not least, the third one is the energy conversion efficiency which is defined as the ratio of the sensible heat of insulation and the LHV of product gas to the sum of simulated solar lights and the LHV of coal, is expressed as:

$$\eta_{energy} = \frac{\int \dot{n}_p LHV_p dt + \int \dot{Q}_{insulation} dt}{\int \dot{Q}_{solar} dt + m_{coal} LHV_{coal}} \quad (5)$$

where $\dot{Q}_{insulation}$ is the sensible heat entering the insulation from the reactor in this setup, and $\dot{Q}_{solar}$ is the simulated solar power input to the reactor.

2.4 Dynamical analysis methods

Thermoanalytical kinetics is a method to study the rate and mechanism of chemical reactions, and the corresponding kinetic parameters can be obtained from kinetic reaction calculations. The gasification reaction in the reactor is a non-homogeneous reaction of solids, and according to the kinetic principle of thermal analysis, the reaction process can be expressed by the following equation

$$\frac{d\alpha}{dt} = f(\alpha) k(T) \quad (6)$$

where α is the conversion rate, t is the reaction time, $k(T)$ is the temperature dependence of the reaction rate constant, $f(\alpha)$ is the conversion function of the reaction.

According to the Arrhenius equation [35], the relationship between the reaction rate and temperature can be expressed as:

$$k(T) = A\exp(-\frac{E}{RT}) \quad (7)$$

where A is the pre-exponential factor, E is the activation energy, T is the reaction temperature, and R is the gas constant (8.314 $J \cdot K^{-1} \cdot mol^{-1}$). By combining eq. (6) and eq. (7), with adding the heating rate (coal gasification reaction is a non-isothermal process), $\beta = \frac{dT}{dt}$, to the combined equation, we can obtain the following equation:

$$\frac{d\alpha}{dt} = \frac{1}{\beta} A\exp(-\frac{E}{RT}) f(\alpha) \quad (8)$$

The single scanning rate method [36] calculates the kinetic parameters according to a non-isothermal thermogravimetric curve, which needs to assume the reaction conversion function. It is also called the hypothetical reaction model method. The widely used single scanning rate method is the Coats-Redfern method [37], which takes that the reaction conversion function is the reaction order model:

$$f(\alpha) = (1-\alpha)^n \quad (9)$$

where n is the order of the reaction.

Li [38] found that the gasification reaction of coal belongs to order one reaction, n = 1, so it can be obtained:

$$\ln\left[\frac{-\ln(1-\alpha)}{T^2}\right] = \ln\left[\frac{AR}{\beta E}\left(1-\frac{2RT}{E}\right)\right] - \frac{E}{RT} \quad (10)$$

In addition, for the activation energy at the general temperature of the gasification reaction, $\frac{E}{RT} \gg 1$, so, $1-\frac{2RT}{E} \approx 1$, substituting it into eq. (10),

$$\ln\left[\frac{-\ln(1-\alpha)}{T^2}\right] = \ln\frac{AR}{\beta E} - \frac{E}{RT} \quad (11)$$

Thus, we can take $\frac{1}{T}$ as the abscissa, and $\ln\left[\frac{-\ln(1-\alpha)}{T^2}\right]$ as the ordinate to plot a fitting line. Then we can calculate the activation energy under a specific heating rate. We optimize the process of the Coats-Redfern method by combining it with the

conversion of the reaction. The kinetic parameters are obtained by fitting within ± 50 K near a specific coal conversion.

2.5 Exergy analysis

To perform a technical evaluation of the hybrid system, we analyzed the exergy of the system. Exergy analysis combines chemical properties with system states (eg, temperature, pressure) to obtain overall exergy efficiency[39].

The solar exergy rate can be computed according to eq. (12) [26]：

$$\dot{E}x_{Sun} = A_d I_b[1 + \frac{1}{3}\left(\frac{T_{amb}}{T_{sun}}\right)^4 - \frac{4}{3}(\frac{T_{amb}}{T_{sun}})] \quad (12)$$

where A_d is the area of the concentrator, I_b is expressed as solar irradiance. T_{amb} and T_{sun} imply to the ambient temperature (details are in Appendix B) and sun temperature (5600 K) respectively.

Meanwhile, the exergy loss including heat transfer, convection, and radiation losses from the solar dish module can be calculated according to eq. (13) [26]：

$$\dot{E}x_{L,Dish} = (1 - \frac{T_{amb}}{T_{gasifier}})\dot{Q}_{L,dish} \quad (13)$$

where $T_{gasifier}$ is the reaction temperature of the gasifier, and $\dot{Q}_{L,dish}$ is expressed as heat loss of solar dish module (details are in Appendix B eq. (B4) to eq. (B13)).

The exergy efficiency of the solar dish module can be formed as follows [40]:

$$\psi_{E,dish} = \frac{P_{dish} - \dot{E}x_{L,Dish}}{\dot{E}x_{Sun}} \quad (14)$$

where P_{dish} implies output power of solar dish module (W).

The state of the coal entering the gasifier is close to the dead state. Thus, the physical exergy of the coal is considered zero. The chemical exergy of the fuel can be computed according to eq. (15) [41]：

$$\dot{E}x_{C,coal} = \dot{m}_{coal} e^{C}_{coal} \quad (15)$$

$$e^{C}_{coal} = LHV[1.0064 + 0.1519\frac{H}{C} + 0.0616\frac{O}{C} + 0.0429\frac{N}{C}] \quad (16)$$

where $\dot{m}_{coal}$ (kg/s) and e^{C}_{coal} (J/g) belong to the fuel mass flow and specific chemical exergy. H, C, O, N is expressed as the mass fraction of elements (details are in Table 1).

The exergy efficiency of the gasifier module can be formed as follows[42]:

$$\psi_{E,gasifier} = \frac{P_{product}}{\dot{E}x_{C,coal}} \quad (17)$$

where $P_{product}$ implies the exergy of gasification products.

The exergy efficiency of the solar coal gasification system can be computed according to eq. (18):

$$\psi_{E,system} = \frac{P_{dish}+P_{product}}{\dot{E}x_{Sun}+\dot{E}x_{C,coal}} \quad (18)$$

This study evaluates the solar coal gasification system with experimental thermodynamics, energy models, and exergy analyses to guide industrial production. The thermodynamic, energy and exergy models used in this study were calculated with homemade MATLAB programs.

2.6 Operational details

Gasification requires a high temperature. We have selected various operating conditions, as shown in Table 2, to ensure that the gasification reaction is thorough enough; and to reduce the temperature drop from the excessive convection heat transfer caused by high-speed flow. Comparing Case 1 and Case 2 reveals the effect of catalyst addition on indirect radiation gasification while comparing Case 1 and Case 3 is to study the differences in radiation forms. Furthermore, comparing Case 4, Case 5, and Case 6 is to study the effect of the ratio of catalysts under direct radiation. And

313 comparing Case 5 and Case 7 is to investigate the effect of catalyst types. *R* is the ratio
314 of catalyst to coal. The experimental mix form is physically mixing.

315 Table 2 Experimental parameters of the solar-driven coal gasification

Case	radiation form	Coal (g)	CO_2(L/min)	N_2(L/min)	Catalyst		*R*
					K_2CO_3(g)	Na_2CO_3(g)	
Case 1	indirect	1	0.05	0.075	0	0	0
Case 2	indirect	1	0.05	0.075	0.1	0	0.1
Case 3	direct	1	0.05	0.075	0	0	0
Case 4	direct	1	0.05	0.075	0.05	0	0.05
Case 5	direct	1	0.05	0.075	0.1	0	0.1
Case 6	direct	1	0.05	0.075	0.2	0	0.2
Case 7	direct	1	0.05	0.075	0	0.05	0.05

316

317 3 Results and discussion

318 3.1 Comparison of direct and indirect radiation gasification

319 N_2 and CO_2 were used to purge the reactor. We started the experiment when the gas
320 components were kept within ±0.1% fluctuations for 10 minutes. We turned on a
321 simulated light at 5 mins intervals during the experimental operation.

322

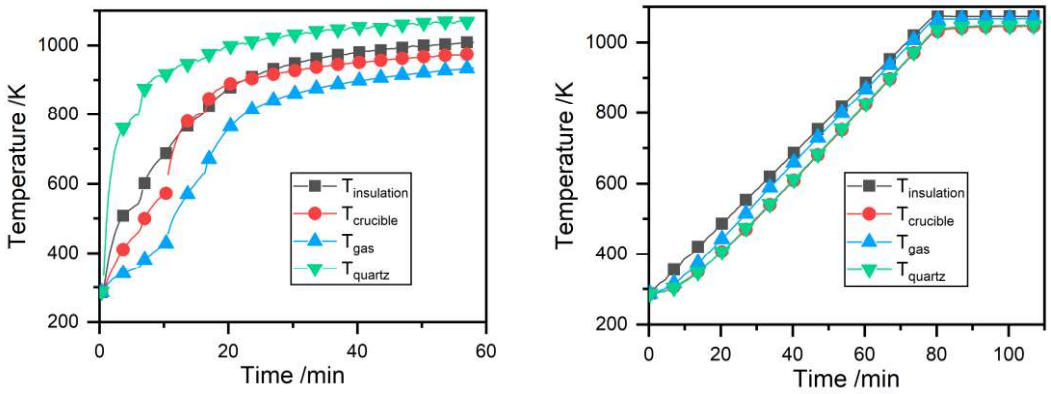

(a) Direct radiation gasification (b) Indirect radiation gasification

Figure 4 Time evolution of temperature

Figure 4 (a) shows the time evolution of the temperature measured by the four Omega k-type thermocouples. The temperature of the quartz tube is always the highest, and the gas temperature is always the lowest. The maximum temperature difference between the two is nearly 400 K. With the advance of time, the temperature of the crucible is first lower than that of the insulation, reaching the same in about 18 minutes, and finally, the two tend to be close.

We use resistance wire heating to simulate indirect radiation gasification. Fig. 4 (b) shows the time evolution of temperature under indirect radiation gasification. The location of the four thermocouples is the same as that of the direct radiation gasification system, but their change trend is different. It can be seen that the difference between the four temperature curves is smaller than that of the direct radiation gasification system. The maximum temperature difference of the four thermocouples at the same time point is about 50 K. Besides, the temperature change trend measured by the four thermocouples is the same, reaching a constant set temperature of 1073 K at the set time.

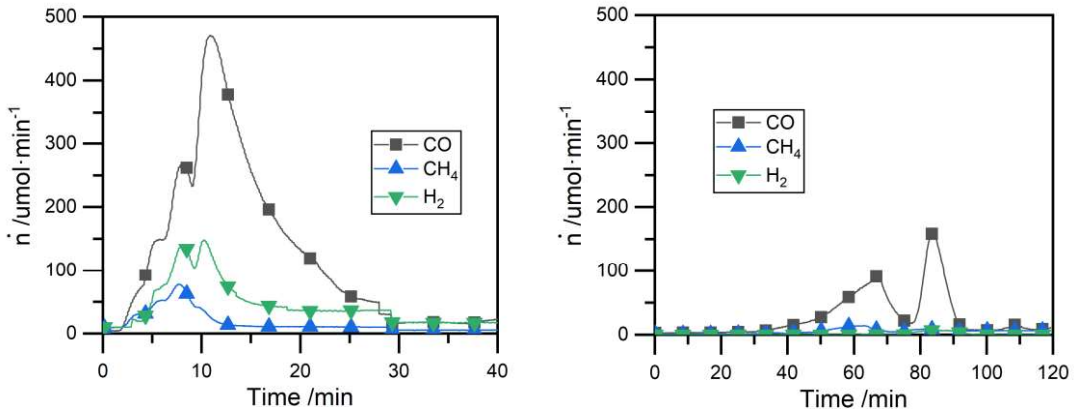

(a) Direct radiation gasification (b) Indirect radiation gasification

Figure 5 Time evolution of molar flow rates

Figure 5 shows the time evolution of products of gas. The gas production rate of the radiation gasification system is the focus of system product analysis. The gasification reaction process of direct radiation and indirect radiation is different. On the one hand, there will be light and heat synergy under the spotlight of four xenon simulated lights for direct radiation gasification. Comparing Fig. 5 (a) and Fig. 5 (b), the time point of the carbon monoxide production of direct radiation gasification is earlier than that of indirect radiation gasification. Moreover, at the same reaction temperature, the amount of carbon monoxide obtained by direct radiation gasification is much higher than that of indirect radiation gasification. There is only one peak under direct radiation gasification from the peak distribution of product gas rate in the reaction process. Komada [13] et al. reported the same distribution under direct radiation gasification.

On the other hand, the coal pyrolysis and the Boudouard reaction under indirect radiation gasification have an apparent time order. Sanchez-Hervas [43] et al. reported that when the temperature reaches about 500 ℃, coal begins to experience pyrolysis, and the carbon monoxide product belongs to the volatile. When the temperature reaches 650 ℃, the coal char reacts with CO_2 and generates more carbon monoxide. This trend

354 is consistent with the experimental results in Fig. 6 (b).

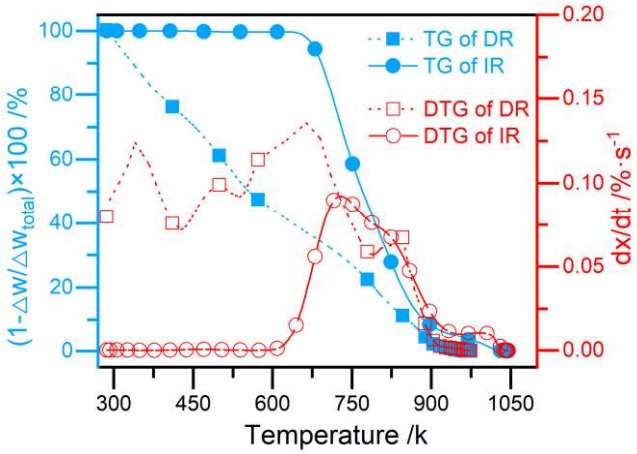

355

356 Figure 6 Reactivity of coal in different radiation forms

357 Figure 6 shows the reactivity of coal under direct radiation (DR) and indirect (IR)
358 radiation based on the thermogravimetric (TG) and differential thermogravimetric
359 (DTG) analysis. It can be seen that the TG curve shifts toward the high-temperature
360 region during indirect radiation and the peak of the DTG curve decreased by 34%.
361 These results indicate that the coal reactivity under indirect radiation is lower than that
362 under direct radiation. This is mainly because the process of devolatilization under
363 indirect radiation gasification is slower, and more volatile components are attached to
364 the coal char surface[44]. The residual volatiles are further removed, and the difference
365 in coal reactivity under indirect and direct radiation becomes smaller with temperature.
366 At the same time, the molecular structure of coal char shifts towards graphitic crystals
367 with temperature, which leads to a decrease in reactivity.

368 3.2 Effects of catalyst types under direct radiation gasification

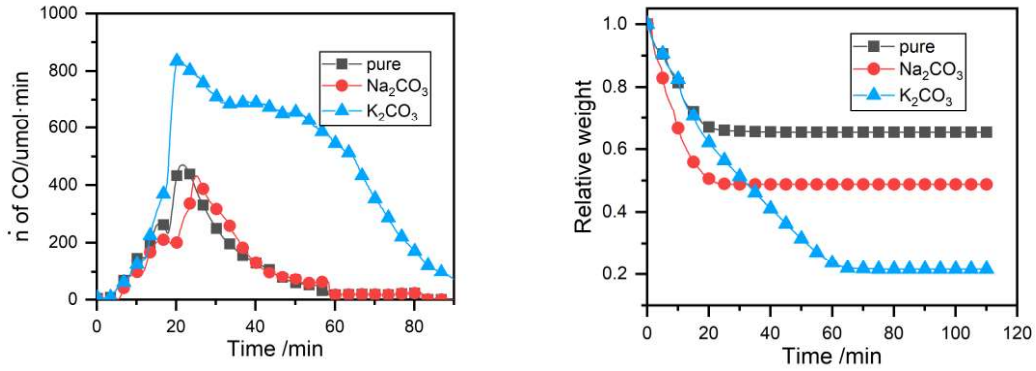

(a) Time evolution of CO molar flow rates

(b) Time evolution of weight loss

Figure 7 Direct radiation gasification characteristics of different catalysts

Fig. 7 (b) shows that radiation gasification cannot reach a high conversion under this temperature (1073.15 K). The means to increase the conversion are high pressure or catalysis. We usually choose to add appropriate catalysts under laboratory conditions. We selected two common catalysts for coal gasification, Na_2CO_3, and K_2CO_3. Fig. 7 (a) shows that the molar flow rate of CO after adding Na_2CO_3 is consistent with the direct radiation gasification without adding any catalyst and reaches the peak at almost the same time point. At the same time, Fig. 7 (b) shows that the conversion rate after adding Na_2CO_3 is higher than that without adding any catalyst, which is about 20%. These results show that the catalytic effect of Na_2CO_3 on the Boudouard reaction is poor in the form of direct radiation gasification at this temperature.

However, the situation is different with K_2CO_3 added. Fig. 7 (a) shows that the peak value of CO molar flow rate with K_2CO_3 is about twice that of the other two groups. Meanwhile, the conversion rate after adding K_2CO_3 is the highest. Thus, we used K_2CO_3 as the catalyst for direct radiation gasification in subsequent experiments.

3.3 Effects of K_2CO_3 on direct or indirect radiation gasification

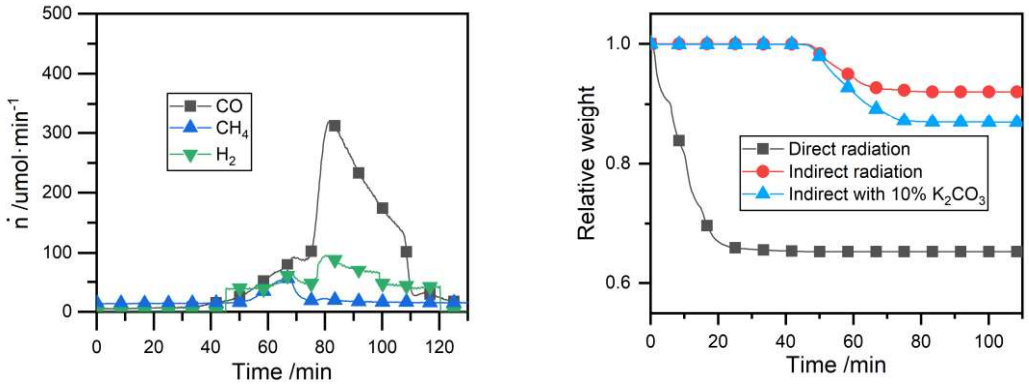

(a) Time evolution of CO production rate (indirect radiation with K_2CO_3)

(b) Time evolution of weight loss

Figure 8 Gasification characteristics of different radiation forms

We also investigate the addition of K_2CO_3 under indirect radiation gasification. The effects of K_2CO_3 and radiation form (direct or indirect radiation) on gasification are compared in the subsequent analysis. Fig. 8 (a) shows the time evolution of gas product rates under indirect radiation with K_2CO_3. Compared to Fig. 5 (b), there is only one peak in CO molar flow rate. This is because the gasification reactivity is strengthened under the catalysis of K^+, and the Boudouard reaction of coal char begins at a lower temperature[32].

However, Fig. 8 (b) shows direct, indirect, and indirect catalytic radiation gasification weight loss. We found that the catalyst can enhance the reactivity of coal gasification and improve coal conversion to a certain extent, but this improvement is limited on indirect radiation form. In Fig. 8 (b), although direct radiation can enhance the reactivity of gasification, the weight loss rate can be further improved. Meanwhile, in Fig. 7 (b), the weight loss rate sees a big increase with the addition of catalyzes on direct radiation form. Therefore, we will add catalysts under direct radiation gasification in the follow-up research. The product's production rate under direct

radiation with K_2CO_3 would be present in the next section.

3.4 Effects of different catalyst ratios on gasification reaction under direct radiation

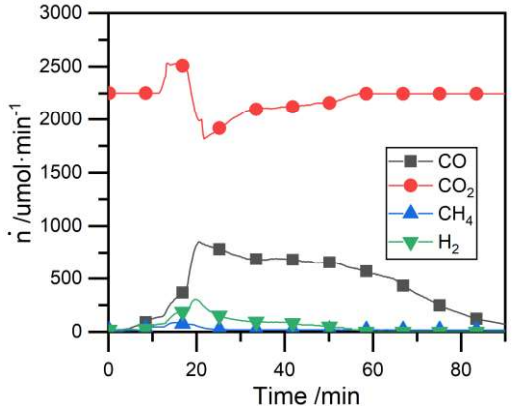

(a) Molar flow rates of the gas in Case 4 (5 % K_2CO_3)

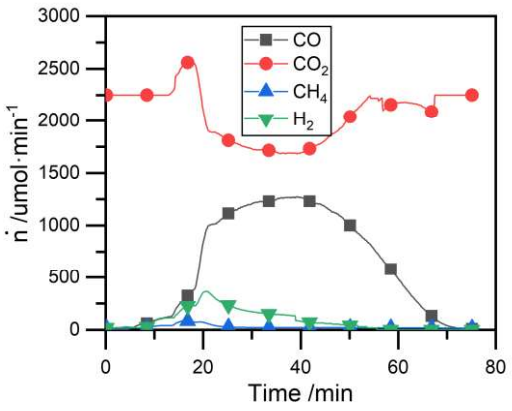

(b) Molar flow rates of the gas in Case 5 (10 % K_2CO_3)

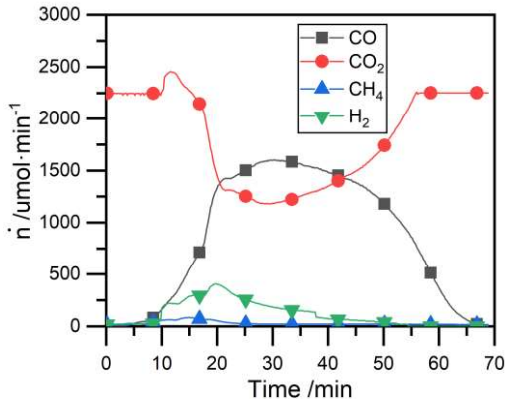

(c) Molar flow rates of the gas in Case 6 (20 % K_2CO_3)

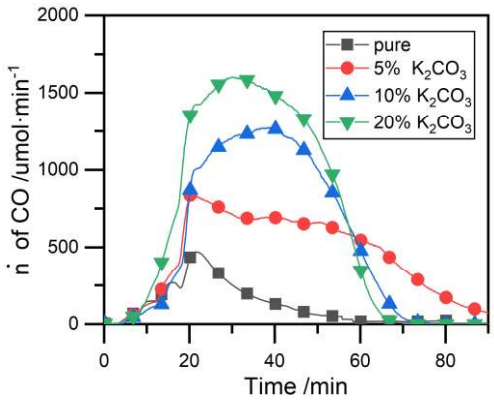

(d) Molar flow rates of CO in cases 3, 4, 5, and 6.

Figure 9 Molar flow rates of the cold product gas in different proportions of catalyst

We investigated the influence of different K_2CO_3 ratios (5%, 10%, and 20%) on gasification distribution. Figure 9 shows the mole flow rates of the gas products in different ratios and the CO molar flow rates comparison of four cases. As shown in Fig. 9 (a), the molar flow rate of CO_2 increases with temperature, marking the beginning of pyrolysis. And the peak value of CO_2 reached about 2500 umol/min with the progress of primary pyrolysis. Then, the gasification reaction (the Boudouard reaction) begins

with the decrease of CO_2, and CO starts to generate, with a peak value of about 800 umol/min. With the progress of the reaction, the coal char is subject to secondary pyrolysis, and the end sign is that the generation of H_2 stops. Fig. 9 (b) shows that the decrease of CO_2 increases with the ratio of K_2CO_3, indicating the rise in the gasification reaction rate. The rate curves of CO_2 and CO intersect in Fig. 9 (c), which means the Boudouard reaction is more intense. Fig. 9 (d) shows that the molar flow rate of CO increases with the addition and ratios of K_2CO_3, and the peak generation rate increases from about 500 umol/min without a catalyst to about 800 umol/min (5 % K_2CO_3), then to about 1650 umol / min (20 % K_2CO_3). The catalytic effect is pronounced. However, the increase in peak value decreases with the ratio of K_2CO_3, which is the same trend as the gasification study of Jan et al. [31]. With the massive use of CO2, the solar gasification system produces chemical feedstocks. This process realizes the low carbon use of coal resources.

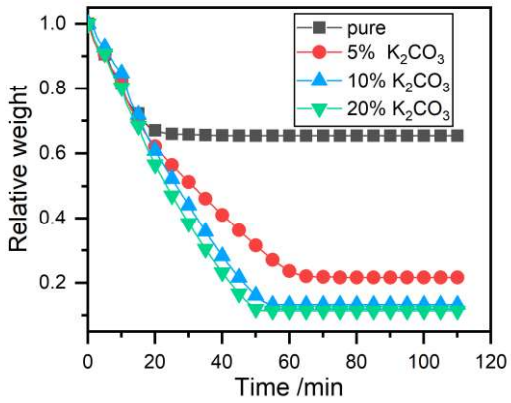

Figure 10 Time evolution of weight loss with different K_2CO_3 ratios

Figure 10 shows the time evolution of different relative weight K_2CO_3 ratios. In combination with the results in Fig. 9 (d) and Fig. 10, the addition of K_2CO_3 can make the Boudouard reaction more thorough and the coal conversion higher. The addition of

catalyst also leads to the Boudouard reaction taking longer than non-K_2CO_3. However, the catalysis Boudouard reaction time is shortened by about 20 mins with K_2CO_3 ratios increase. Comparing the thermogravimetric and molar flow rates of CO in Fig. 9 (d) and Fig. 10, 20 % K_2CO_3 can only improve a few compared to 10 % K_2CO_3. These results mean that 10 % K_2CO_3 can make gasification thorough.

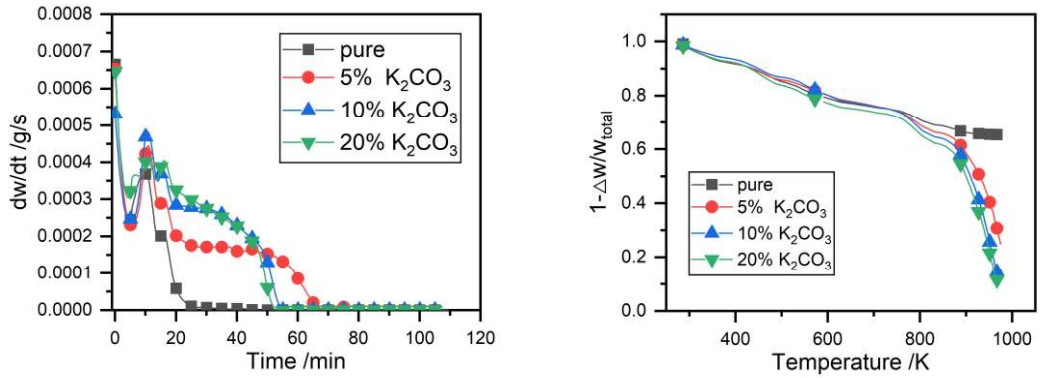

(a) Time evolution of weight loss rates (b) Temperature evolution of weight

Figure 11 Kinetic with different K_2CO_3 ratios

Fig. 11 (a) shows the time evolution of weight loss rates with different K_2CO_3 ratios. All four curves see decreases immediately at the beginning of the devolatilization reaction. After removing volatiles, CO_2 enters the coal char particles for a gas-solid two-phase reaction. The progress of the Boudouard reaction will lead to the consumption of the solid components of the coal char and expose more pores in the coal char. The gas-solid contact area increases with pore size, and the specific surface area of the Boudouard reaction increases. Therefore, the weight loss rate increases at this stage. When the Boudouard reaction proceeds to a certain extent, the consumption of coal char substantially decreases, and the gas-solid contact area decreases gradually. The specific surface area and reaction rate of the Boudouard reaction are reduced with the crosslinking or collapse of the pore structure in the coal char. Besides that, K_2CO_3

has no catalytic effect on the devolatilization reaction. Sharma[45] et al.investigated the relationship between coal gasification reactivity and catalyst addition. The experimental results show that the gasification reactivity of coal char increases with catalyst addition, but there is an optimal addition. When the optimum addition amount is higher than that, the activity of the excess catalyst decreases because their mutual accumulation will increase the average particle size of coal char but reduce the contact area of the coal char surface.

Fig. 11 (b) shows the temperature evolution of weight loss with different K_2CO_3 ratios. When the temperature reaches 750 K, the decreasing slopes of the four curves increase—the gasification reaction stage at this temperature. The pure coal curve has a minor descending slope and the smallest descending magnitude. However, direct radiation catalytic gasification is remarkable. As the catalyst addition ratio increased from 5% to 10%, the volume of the decrease also increased. However, the improvement was limited when the catalyst ratio was increased from 10% to 20%. At the same time, we can also see from Fig. 11 (b) that the separate temperature between the pure curve and the others is about 900 K, which indicates that the K_2CO_3 starts to catalyze at about 900 K.

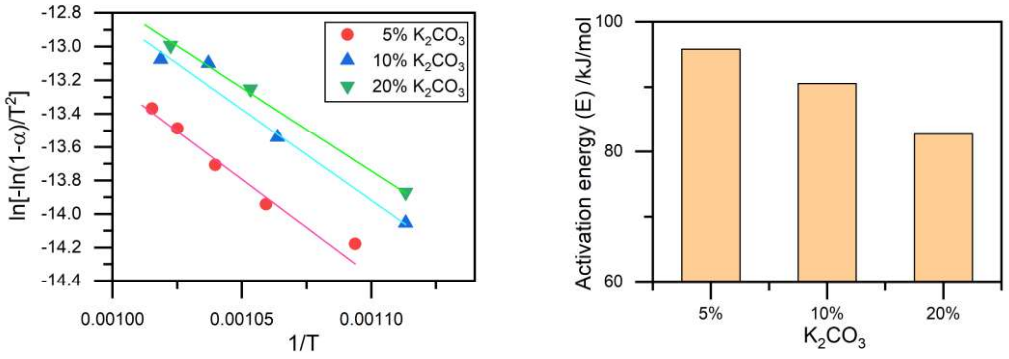

(a) Arrhenius plot (b) Comparison of different ratios

Figure 12 Kinetics analysis at cases 4, 5, and 6

460 Figure 12 shows kinetic analysis using the Coats-Redfern method for different
461 catalyst ratios (5%, 10%, and 20%) of direct radiation catalytic gasification. Fig. 12 (a)
462 shows the fitting Arrhenius plot for cases 4, 5, and 6. The activation energy obtained is
463 95.81 kJ/mol, 90.54 kJ/mol, and 82.86 kJ/mol in Fig. 12 (b).

464 In the initial reaction stage, the temperature is low, but the heating rate is high, and
465 the volatiles will be rapidly removed. During the second half of the reaction, the coal
466 char and catalyst undergo the typical behavior of pore development during coke
467 conversion, which can lead to higher surface area and faster rates. And the activation
468 energy decreases with the catalyst ratio. At higher conversion rates, the gasification rate
469 decreases due to pore collapse and larger potassium clusters. The latter is formed as the
470 surface carbon is released as carbon monoxide gas, and the amount of potassium
471 relative to the carbon increases. The release of residual volatiles, the diffusion of
472 reactive gases, and the expansion of porosity in the coal char all affect the activation
473 energy distribution of gasification.

474 4 Analysis of radiation gasification performance indicators

475 4.1 Element C conversion rate

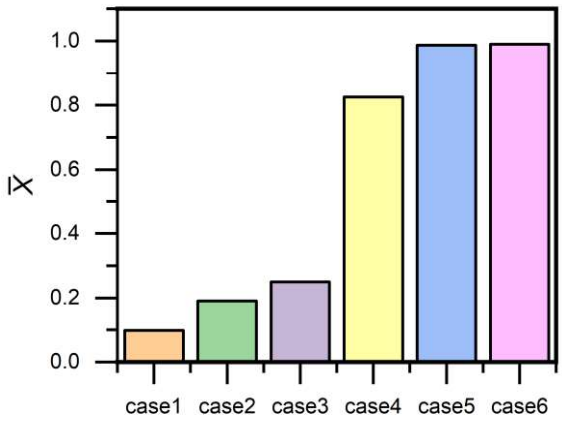

Figure 13 Distribution of elemental C conversion rate

As shown in Fig. 13, we investigate the conversion degree of the coal during radiation gasification by the conversion rate of the C element. The conversion rate of the C element in Case 1 is 0.098. And the conversion rate of Case 3 is 0.25, which is about 2.5 times that of Case 1. The catalyst further improved the C element conversion rates, and the rates of cases 4-6 were 0.825, 0.987, and 0.99, respectively. Case 2 is indirect radiation catalytic gasification, but it is only 0.19. These results show that direct radiation is more effective. The introduction of catalyst alone cannot directly improve the conversion of C element with indirect radiation. The synergistic effect of light and catalyst can significantly improve the conversion of the C element at this temperature.

4.2 Energy conversion efficiency

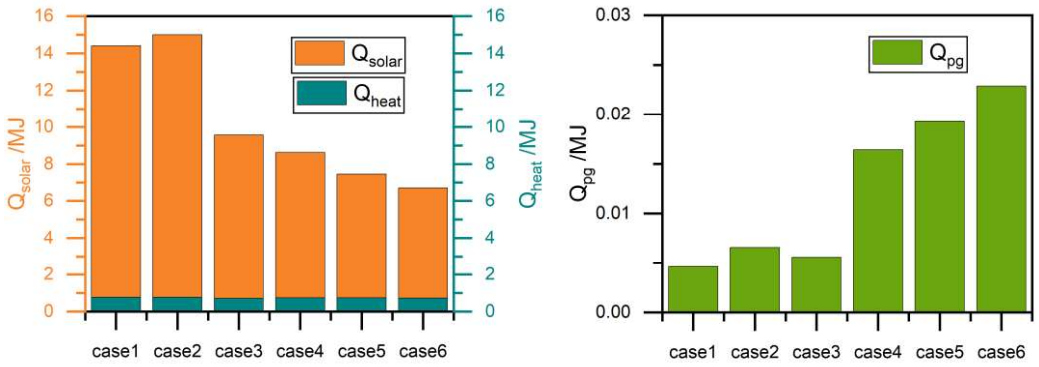

Figure 14 (a) Solar energy and sensible heat

Figure 14 (b) The heat value of the product gas

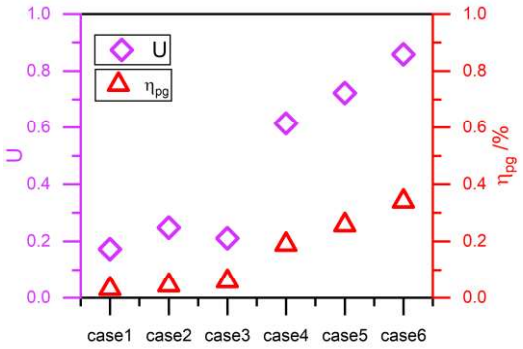

Figure 14 (c) U and η_{pg}

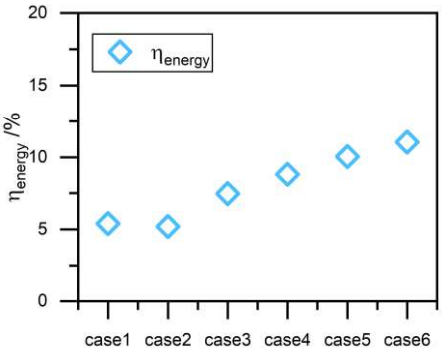

Figure 14 (d) Energy conversion efficiency

Figure 14 System energy distribution

Figure 14 shows the radiant gasification system's energy, including the insulation's sensible heat (Q_{heat}), the heat value of the product gas (Q_{pg}), and the input solar energy (Q_{solar}). At the same time, we calculated energy conversion efficiency (η_{energy}), product gas energy efficiency (η_{pg}) and energy upgrade factor (U).

Indirect radiation gasification (Case 1 and Case 2) requires more solar energy due to its long reaction time. The reaction time for direct radiation gasification is shortened with the catalyst addition. The required solar energy input is also reduced to 6.25 MJ in Figure 14 (a). The catalyst can improve Q_{pg} of indirect radiation gasification (Case 2), but under the synergistic effect of direct radiation (Case 5), Q_{pg} will see a significant increase, about three times that of Case 2 in Figure 14 (b). For Q_{heat}, the temperature rises of each working condition are the same, and there is little difference.

The solar system efficiency under direct radiation gasification will increase from 5.39 % (Case 1) to 7.47 % (Case 3) in Figure 14 (d). The addition of catalysts will further advance this trend, reaching a maximum level of 11%. The trend of product gas

efficiency is similar to solar system efficiency, which is also greatly improved by the synergistic effect of direct radiation and catalyst. Compared with the conversion rate of the C element, the energy upgrade factor is to analyze the radiation gasification system from the perspective of energy. Adding a catalyst can improve the energy upgrade factor of indirect radiation gasification. Direct radiation gasification can also enhance the energy upgrade factor, which indicates that radiation's incoming form will affect energy absorption and utilization. At the same time, in the form of direct radiation, the addition of a catalyst can significantly improve the energy upgrade factor. Moreover, the increase ratio is proportional to the ratio of catalyst, and the highest can reach about 0.86 in Figure 14 (c). The data in Figure 14 are only for the analysis of the experimental process and evaluation. The solar energy entering the gasifier is converted into forms such as chemical energy, which is the storage process of solar gasification. This process is an important means of low carbon use of coal resources.

5 Chemical process analysis

5.1 Energy analysis

We set up three model forms: indirect radiation, direct radiation, and direct catalytic radiation gasification, to investigate the feasibility of applying solar heat sources in the actual coal gasification chemical process. In the actual process, the forms of solar energy utilization include tower type, trough type, and dish type. For the coal gasification chemical process, the disc type has the advantages of flexible installation, concentrated light spot energy, and high temperature, convenient for installation in various terrain. Therefore, we use the dish type to collect and utilize solar energy and

analyze the chemical process energy and exergy. For the whole system, we consider the energy loss of each part. See the calculation process in Appendix B for details. At the same time, we use the corresponding experimental conditions for different systems to predict the product distribution and then carry out the model calculation of coal gasification reaction. At the same time, we compare the overall efficiency of the three systems and the receiver dish area of the disc system.

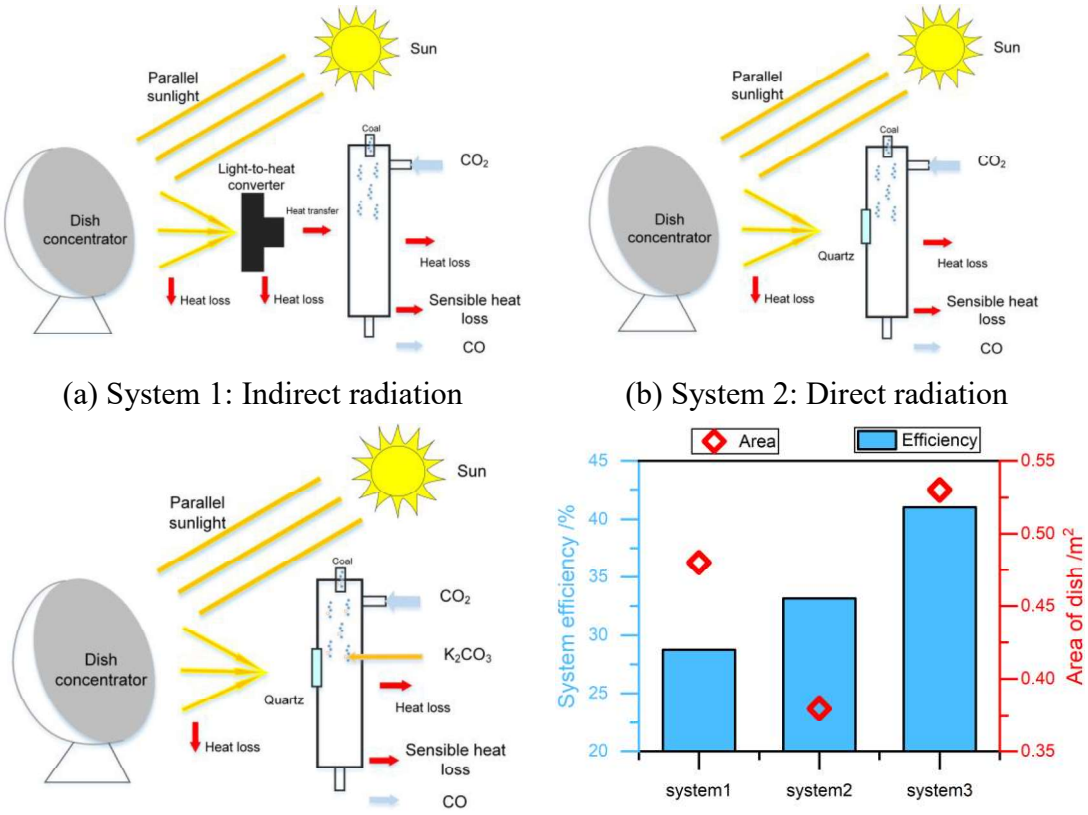

(a) System 1: Indirect radiation (b) System 2: Direct radiation

(c) System 3: Direct catalytic radiation (d) Systems comparison

Figure 15 Different solar energy coal gasification systems

Table 3 Experimental gas products distribution

Products	Volume distribution (%)			Mass distribution (%)		
	System 1	System 2	System 3	System 1	System 2	System 3
CO	68.16	56.22	68.74	66.60	66.73	70.22
CH_4	12.68	7.64	2.30	7.08	5.19	1.34
H_2	2.12	22.08	11.77	0.15	1.87	0.859
CO2	17.04	14.05	17.19	26.17	26.21	27.58

Fig. 15 shows three radiation coal gasification systems and their comparison.

According to the experimental data above, the gas product distribution is in Table 3. For System 1, the heat loss from the concentrator to the reactor was considered. The input coal rate is 135.05 g/h (1 kW heat value). With the same gasification agent and coal ratio as the experiment, the flow rate of CO_2 is 405 L/ h, and the flow rate of N_2 is 607.5 L/h. Estimate the sensible heat loss carried by gases at 800 ℃, referring to the heat value of various gases in [46]. The heat at the reactor output is expressed as

$$\dot{Q}_{output} = \dot{Q}_{sensible} + \dot{Q}_{pg} \tag{19}$$

where $\dot{Q}_{output}$ is the output total heat rate, $\dot{Q}_{sensible}$ is the sensible heat rate, and $\dot{Q}_{pg}$ is the low heat value rate of gas products.

(a) First of all, in System 1:

$$\dot{Q}_{output} = 492.32 \text{ W}$$

The heat rate required by the gasifier is

$$\dot{Q}_{gasifier} = \dot{Q}_{output} + \dot{Q}_{wall} \tag{20}$$

where $\dot{Q}_{wall}$ is the heat loss through the wall, and it is 1.7% of $\dot{Q}_{coal}$ [47]. Then reverse the solar input energy. The system efficiency can be expressed as follows:

$$\eta_{system} = \frac{\dot{m}_p LHV_p}{\dot{Q}_{solar} + \dot{m}_{coal} LHV_{coal}} \tag{21}$$

The efficiency from obtaining solar energy to input energy into the reactor (η_{SE}) is 75.31 %, the system efficiency (η_{system}) is 28.76 %, and the dish area (s) is 0.48 m^2.

(b) Secondly, in System 2:

There is no converter in System 2. Thus, the energy calculation does not consider the converter's transfer and radiation energy loss. We assume that the absorption coefficient of coal is 0.9. We think that the temperature in the reactor is the same as in System 1.

$$\dot{Q}_{output} = 522.77 \text{ W}$$

The system efficiency (η_{system}) is 33.15 %, and the dish area (s) is 0.38 m^2.

(c) Last but not least, in System 3:

The gasification in System 3 is direct radiation with K_2CO_3 addition.

$$\dot{Q}_{output} = 723.58\ W$$

The system efficiency (η_{system}) is 41.04 %, and the dish area (s) is 0.53 m^2.

Fig. 15 (d) compares three different systems on efficiency and the dish area. Under the premise of ensuring the same reactor temperature, direct radiant gasification can obtain higher system energy conversion efficiency. Simultaneously, adding a catalyst can further increase this advantage. Industrial production is often accompanied by large-scale production. Considering the economics of construction, the area of the dish is an important reference indicator. Compared with System 1 and System 3, the dish diameter increases by 5 %, but the efficiency increases by 13 %. The greatly improved system efficiency can further enhance the economic benefits of the large-scale chemical process.

5.2 Exergy analysis

This work investigates the exergy analysis in the solar gasification chemical process, which include the solar concentrator, coal gasifier, and the whole system. The exergy efficiency of different modules provides a reference for the solar gasification chemical process.

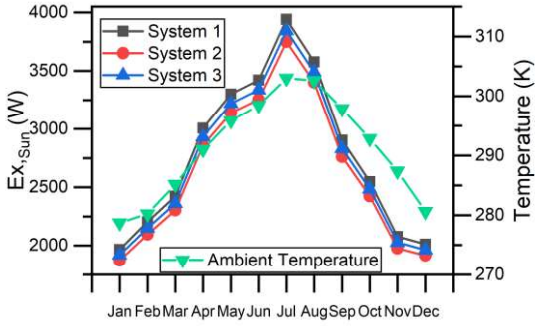

(a) The monthly evolution of the solar exergy and ambient temperature

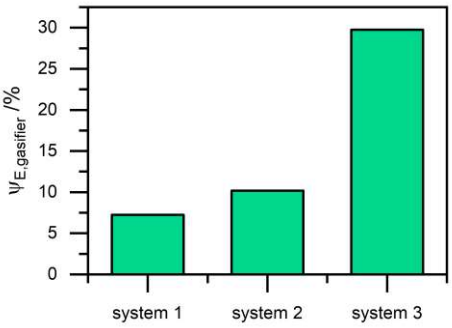

(b) The gasifier exergy efficiency of different systems

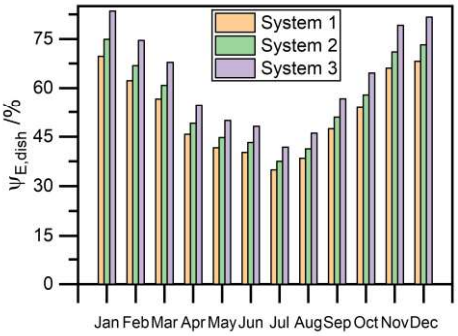

(c) The monthly evolution of the solar dish exergy efficiency

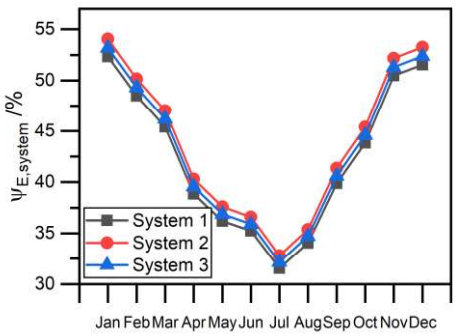

(d) The monthly evolution of system exergy efficiency

576 Figure 16 The module exergy analysis results

577 Fig. 16 (a) shows the monthly evolution of solar dish module exergy analysis and
578 ambient temperature[48]. The solar dish module exergy relates to the ambient
579 temperature. It reaches its peak in summer (3941.18 W/m^2), and the least value of
580 exergy content belongs in December (1871.57 W/m^2). This trend is similar to the solar
581 power module in Ref. [26]. The areas of different systems in the exergy analysis are
582 calculated in Section 5.1 which meets the thermal power needed by the gasifier. The
583 area of the solar dish influences the solar exergy according to eq. (12). The value of
584 solar exergy in system 1 is the highest, as well as that in system 2, which is the least
585 due to different dish areas in the same month. Fig. 16 (b) shows the gasifier exergy
586 efficiency in different systems. The gasifier exergy efficiencies are influenced by the

product distribution and gasification efficiency. It can be concluded that the highest amount of gasifier exergy efficiency belongs to the direct catalytic radiation gasification (system 3, 29.7 %). Fig. 16 (c) shows the monthly evolution of the solar dish exergy efficiency. It can be seen that exergy efficiency decreases with an increase in thermal losses. This law is in good agreement with the values reported in Ref [49]. Fig. 16 (c) also shows that the chemical process of solar gasification needs to be considered with the impact of seasons. This chemical process includes not only the influence of reaction temperature but also the influence of ambient temperature with effects on the exergy efficiency of solar modules. For any month, System 3 always had the highest exergy efficiency of solar modules.

Fig. 16 (d) shows the monthly evolution of the system exergy efficiency in different solar gasification systems, the trend of which is similar to the study [26]. The reason for the decrease in summer is the increase in entropy caused by higher temperature, but the gasifier exergy remains unchanged, resulting in an increase in the exergy loss of the system and a decrease in the exergy efficiency. The highest amount of system efficiency belongs to system 2, as well as the least to system 1.

On one hand, the energy efficiency and the exergy efficiency calculated in the solar dish module of this study are 70 % and 35 – 55 %, respectively. Kasaeian [50] et al. investigated the concentrated solar dish system considering the same heat loss as this work and the same work fluids. They concluded that the energy efficiency is around 70 % and the exergy efficiency is above 30 % in the solar dish system. On the other hand, Table 3 shows the distribution of the products in this work which is within the

609 range of direct radiation gasification at the same temperature studied by Kodama [51]
610 et. al and the range of indirect radiation gasification studied by Li [52] et. al. Meanwhile,
611 the system energy efficiency is improved from 37.2 % in the Ref. [52].

612 6 Conclusion

613 In summary, this work designed a novel experimental solar radiation gasification
614 thermogravimetric device. Furthermore, this work set up a solar gasification system
615 energy and exergy analysis model. With the technological analysis of thermodynamics,
616 energy, and exergy, this work investigated the performances of different radiation forms
617 on solar catalytic gasification. Besides that, this work studied the energy and exergy
618 efficiency of the solar, gasifier module, and the system, respectively. With thermal from
619 solar energy, coal and CO_2 are used as reactants, and the products are used in the
620 chemical industry. This chemical process is an important industrial approach to the low-
621 carbon use of coal resources. Limited by the experimental conditions, the economic
622 analysis of different CO_2 mass flow radiation catalytic gasification will be investigated
623 in the future to meet industrial production. The specific main results are as follows:

624 (1) Direct radiation gasification can improve the average carbon conversion rate. This
625 work compares two radiation forms: direct and indirect radiation gasification. It was
626 found that the carbon conversion rate of direct radiation was 15.2 % higher than that of
627 indirect radiation gasification. Meanwhile, the energy conversion efficiency was
628 increased by 3.73 %.

629 (2) The reaction degree is more intense with high gas production rate under direct
630 radiation gasification. From the kinetic analysis, the TG curve of direct radiation

gasification decreases more rapidly at the same temperature, and the DTG curve shifts upward by 34%.

(3) Only adding catalysts cannot solve the low efficiency of indirect radiation gasification at this experimental condition. Catalyst addition can only increase the weight loss rate of indirect radiation from 8 % to 13.2 %, but that of direct radiation is 34.65 %. The addition of catalyst and direct radiation can significantly improve the efficiency of coal gasification. In direct catalytic radiation gasification, the weight loss reaches up to 90 % with the synergistic effect of light and heat (the remaining is ash).

(4) Meanwhile, this work investigates the catalyst ratios in kinetics under direct catalytic radiation gasification. It was found that the 10% ratio is more suitable for system analysis. Direct catalytic radiation at a lower gasification temperature (800 °C) can improve the carbon conversion to 99 %, the energy upgrading factor to 0.86, and the energy conversion efficiency to 11 %.

(5) In dish-type concentrated solar systems, solar and catalyst synergistic effects can increase system efficiency up to 41%. Compared to indirect radiation, direct radiation catalytic gasification increases the dish diameter by only 5% but the efficiency by 13%. The gasification conditions are often harsh (high temperature and pressure). But the direct radiation system and catalyst will allow solar coal thermochemical conversion to be available.

(6) Solar irradiation and ambient temperature can affect the solar dish exergy. Meanwhile, the catalysis addition and the direct radiation form can improve the value of the exergy efficiency of solar coal gasification. The solar dish exergy reaches its peak

in summer (3941.18 W/m^2), and the least value of exergy content belongs in December (1871.57 W/m^2). The highest amount of gasifier exergy efficiency belongs to the direct catalytic radiation gasification (system 3, 29.7 %), as well as the least value of gasifier exergy efficiency implies indirect radiation gasification (system 1, 7.23 %). These results will potentially improve the popularity of new energy sources and the efficiency of resourceful and low-carbon utilization of coal in chemical process.

Acknowledgments

The work is financially supported by the Science and Technology Department of Ningxia Province (No. 2018BCE01004), the National Postdoctoral Program for Innovative Talents of China (BX2021254), China Postdoctoral Science Foundation (2021M702793), and the China Scholarship Council (202106320152).

Appendix A

A.1 Reactor

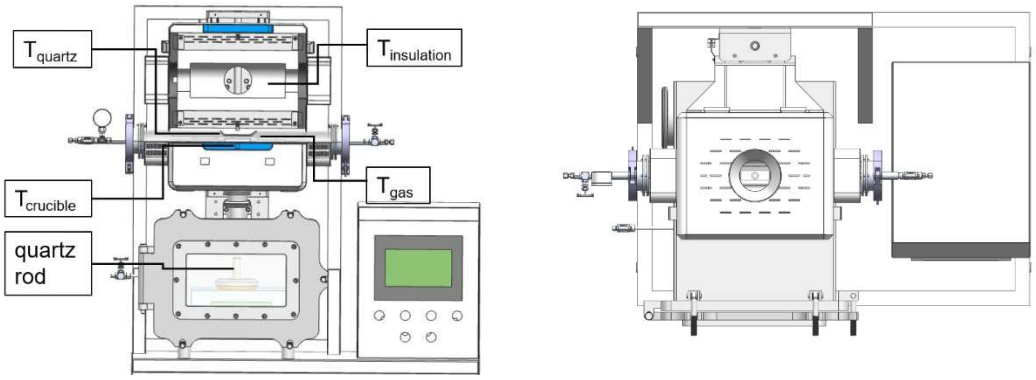

(a) Main view (b) Top view

Figure A1 Reactor

The reactor in the radiation gasification-thermogravimetric test bench based on full-

spectrum concentrated solar energy is shown in Figure A1 (a). Figure A1 (b) shows the top view after the covered insulation. The core reaction zone is made of quartz. The insulation material adopts alumina fiber, which has the characteristics of low thermal conductivity, and thermocouples are arranged in the insulation. The upper part of the insulation is drilled to inject the simulated solar light at a specific angle, and the shell is supported by 5 mm stainless steel (SS304). The T-tube is smoothed in the area irradiated by the simulated sunlight. At the same time, the T-tube is connected to the thermogravimetric chamber. There is an analytical balance with a range of 0-220g and an accuracy of 0.001g in the room. We put a quartz rod to jack up the crucible made of Al_2O_3 to connect the balance and the crucible. N_2 flows into the left side of the thermogravimetric chamber to avoid high-temperature damage to the electronic balance.

A.2 Optical power of simulated solar lights

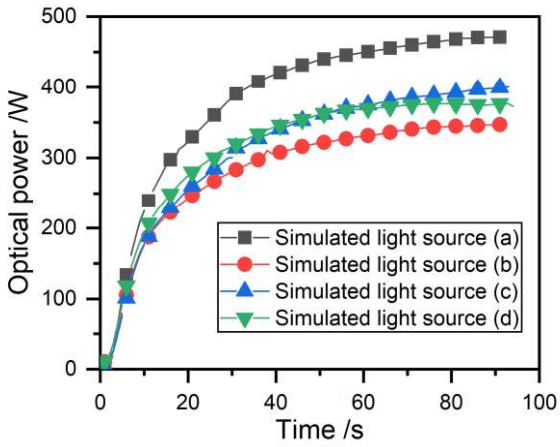

Figure A2 Time evolution of simulated lights' power

The spot power of the xenon lamp irradiated to the crucible was measured using an optical power detection device, HP100A-4KW-HE, provided by Gentec, and Figure A2 shows the measurement results. After 80 s of irradiation, all four simulated lights (a, b,

c and d) reached a steady state. The radiation power delivered to the radiation gasifier needs to be adjusted in a typical radiation gasification experiment. The heat stages include preheating, rated heating, and steady-state heating in sequence. The calculation gives a total simulated solar radiation input power of 1594.44 W

Appendix B

Appendix B introduces the calculation process of the energy analysis model and the monthly evolution solar irradiation model of solar concentrating radiation gasification.

B.1 Energy analysis model

Assume that the average input of the sun to the dish concentrator is 1000W/m^2 [7]:

$$G = 1000\ W/m^2 \tag{B1}$$

The focal length (f) and condensing ratio (C) are calculated as follows [53]:

$$f = \frac{d_d}{4\tan(\psi_{rim/2})} \tag{B2}$$

$$\mathrm{C} = (\frac{d_d}{d_{ap}})^2 \tag{B3}$$

where d_d is the diameter of the dish, d_{ap} is the diameter of the aperture, ψ_{rim} is the rim angle.

Dish solar concentrators use a dual-axis tracking mechanism that continuously tracks the sun to collect maximum sunlight, so the angle of incidence is always equal to zero.

Table B1 The technical specifications of solar collector

System	f	C	Operating type
System 1	0.47	243.36	Dual-Axis mode
System 2	0.42	196.00	Dual-Axis mode

System 3	0.49	268.96	Dual-Axis mode

In our model, the collection and gasifier are integrated, so that the collection temperature is the same as the gasification temperature (1073 K), which is determined. Meanwhile, the concentration ratios used were 243.36, 196.00, and 268.96, respectively. With the same collection temperature and similar concentration, the energy efficiency can be compared to show the catalyst performance. The collection efficiency of systems is 62.2 %, 55.49%, and 64.85 %, respectively. The effect of concentration ratio is included in the system efficiency as a dependent variable, not an independent variable.

Convective heat transfer coefficient through the receiver cavity, Nussle number natural convective heat transfer coefficient, forced convective heat transfer coefficient, and total convective heat transfer coefficient are expressed as [54]:

$$\mathrm{Nu}_{natural} = 0.088 \cdot Gr^{1/3} \cdot \left(\frac{T_{cav}}{T_{amb}}\right)^{0.18} \cdot (cos\theta)^{2.47} \cdot \left(\frac{d_{ap}}{d_{cav}}\right)^{-0.982 \cdot \left(\frac{d_{ap}}{d_{cav}}\right) + 1.12} \quad \text{(B4)}$$

$$\mathrm{h}_{forced} = 0.1967 \cdot v^{1.849} \quad \text{(B5)}$$

$$\mathrm{h}_{total} = \mathrm{h}_{natural} + \mathrm{h}_{forced} \quad \text{(B6)}$$

where Gr is Grashov number, T_{cav} is the temperature of the receiver cavity, T_{amb} is the temperature of ambient, θ is the incident angle, v is the wind speed (m/s).

Reflected and emitted radiative heat transfer from the receiver cavity:

$$\dot{\mathrm{Q}}_{reflected} = (1 - \alpha_{eff}) \cdot \eta_{conc} \cdot G \cdot \mathrm{A}_d \quad \text{(B7)}$$

$$\dot{\mathrm{Q}}_{emitted} = \varepsilon \cdot A_{ap} \cdot \sigma(T_{cav}^4 - T_{amb}^4) \quad \text{(B8)}$$

Where

$$\alpha_{eff} = \alpha_{eff}/[\alpha_{cav} + (1 - \alpha_{cav})/(A_{ap}/\mathrm{A}_{cav})] \quad \text{(B9)}$$

α is the absorptivity, A is the area, and η_{conc} is the efficiency of the concentrator.

The conduction, convection, radiation, and total heat losses of the receiver are expressed as:

$$\dot{Q}_{conduction} = \frac{T_{cav} - T_{amb}}{\ln\left[\frac{\frac{d_{cav}}{2} + \delta_{insul}}{\frac{d_{cav}}{2}}\right] / (2\pi k_{insul} L_{cav})} \quad \text{(B10)}$$

$$\dot{Q}_{convection} = h_{total} \cdot A_{cav} \cdot (T_{cav} - T_{amb}) \quad \text{(B11)}$$

$$\dot{Q}_{radiation} = \dot{Q}_{reflected} + \dot{Q}_{emitted} \quad \text{(B12)}$$

$$\dot{Q}_{L,dish} = \dot{Q}_{conduction} + \dot{Q}_{convection} + \dot{Q}_{radiation} \quad \text{(B13)}$$

where δ_{insul} is the thickness of insulation.

The efficiency of the receiver is calculated as

$$\eta_{rec} = 1 - \frac{\dot{Q}_{total}}{\eta_{conc} \cdot G \cdot A_d} \quad \text{(B14)}$$

The energy input to the coal gasification reactor is

$$\dot{Q}_{input} = \eta_{rec} \cdot \eta_{conc} \cdot G \cdot A_d \quad \text{(B15)}$$

The heat loss through the wall is about 1.7% of the heat value of coal input [29]:

$$\dot{Q}_{wall} = 17\ W \quad \text{(B16)}$$

Sensible heat loss in output gas [46]：

$$\dot{Q}_{sensible} = (\dot{m}_{CO} \cdot c_{CO} + \dot{m}_{CO_2,out} \cdot c_{CO_2} + \dot{m}_{CH_4} \cdot c_{CH_4} + \dot{m}_{H_2} \cdot c_{H_2} + \dot{m}_{N_2} \cdot c_{N_2}) \cdot T_{output} \quad \text{(B17)}$$

$$\dot{Q}_{pg} = \dot{m}_p LHV_p \quad \text{(B18)}$$

where T_{output} is the temperature of the reactor export, $\dot{m}$ is the mass flow, and c is the specific heat capacity.

The specific heat capacity is expressed as:

$$C_{p_i} = a + bT + cT^2 + dT^3 \quad \text{(B19)}$$

where a, b, c, and d are the specific gas product specific heat capacity coefficient[55].

B.2 The monthly evolution solar irradiation model

The solar irradiation outside the earth (G_{on}) is expressed according to eq. (B20) [56]：

$$G_{on} = G_{SC}(1.000110 + 0.034221cosB + 0.001280sinB + 0.000719cos2B +$$

$$0.000077sin2B) \quad \text{(B20)}$$

where G_{SC} is the solar constant ($1367\ W/m^2$), $B = (n-1) \times 360/365$, n is the n-th of one year.

The declination angle (δ) is expressed according to eq. (B21) :

$$\delta = (\frac{180}{\pi})(0.006918 - 0.399912cosB + 0.070257sinB - 0.006758cos2B + 0.000907sin2B - 0.002697cos3B + 0.00148sin3B) \quad \text{(B21)}$$

The zenith angle (θ_z) is expressed according to eq. (B22):

$$cos\theta_z = cos\varphi cos\delta cos\omega + sin\varphi sin\delta \quad \text{(B22)}$$

where φ is the latitude (°), and ω is the time angle (°).

The atmospheric transmittance (τ_b) is expressed according to eq. (B23):

$$\tau_b = a_0 + a_1 \exp\left(-\frac{k}{cos\theta_z}\right) \quad \text{(B23)}$$

where a_0, a_1 are the constant of the atmospheric transmittance formula, and k is thermal conductivity ($W/(m \cdot K)$)

Solar irradiation (I_b) on inclined surfaces can be expressed according to eq. (B24):

$$I_b = G_{on}\tau_b cos\theta \quad \text{(B24)}$$

where θ is the incidence angle (°).

Dish solar concentrators use a dual-axis tracking mechanism that continuously tracks the sun to collect maximum sunlight, so the angle of incidence is always equal to zero ($cos\theta = 1$).

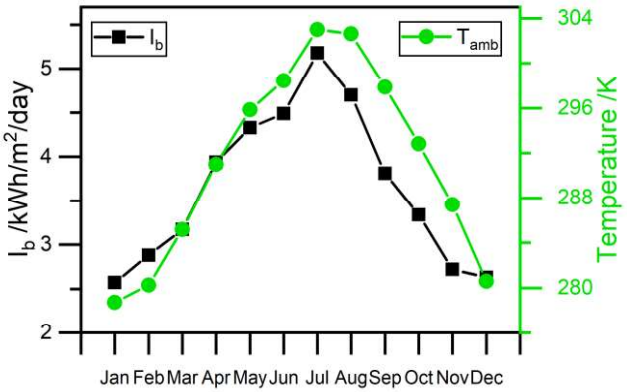

773

774 Figure B1 The monthly evolution of I_b and T_{amb}.

775 With this calculation process, Figure B1 shows the monthly evolution of solar

776 irradiation. Meanwhile, we obtain the monthly evolution of ambient temperature in

777 Hangzhou on the website [48].

778

References

[1] T. Wilberforce, A.G. Olabi, E.T. Sayed, K. Elsaid, M.A. Abdelkareem, Progress in carbon capture technologies, Sci. Total Environ. 761 (2021) 143203. https://doi.org/10.1016/j.scitotenv.2020.143203.

[2] X. Zhao, X. Ma, B. Chen, Y. Shang, M. Song, Challenges toward carbon neutrality in China: Strategies and countermeasures, Resour. Conserv. Recycl. 176 (2022) 105959. https://doi.org/10.1016/j.resconrec.2021.105959.

[3] Z. Zhou, L. Guo, L. Chen, S. Shan, Z. Wang, Study of pyrolysis of brown coal and gasification of coal-water slurry using the ReaxFF reactive force field, Int. J. Energy Res. 42 (2018) 2465–2480. https://doi.org/10.1002/er.4029.

[4] D. Yadav, R. Banerjee, A review of solar thermochemical processes, Renew. Sustain. Energy Rev. 54 (2016) 497–532. https://doi.org/10.1016/j.rser.2015.10.026.

[5] J.W.K. Norman C. Ford, Solar Power, Bull. At. Sci. 3402 (1971) 1–27. https://doi.org/10.1080/00963402.1971.11455398.

[6] S. Abanades, P. Charvin, G. Flamant, P. Neveu, Screening of water-splitting thermochemical cycles potentially attractive for hydrogen production by concentrated solar energy, Energy. 31 (2006) 2805–2822. https://doi.org/10.1016/j.energy.2005.11.002.

[7] A. Steinfeld, Solar thermochemical production of hydrogen - A review, Sol. Energy. 78 (2005) 603–615. https://doi.org/10.1016/j.solener.2003.12.012.

[8] A. Kogan, Direct solar thermal splitting of water and on-site separation of the products - IV. Development of porous ceramic membranes for a solar thermal water-splitting reactor, Int. J. Hydrogen Energy. 25 (2000) 1043–1050. https://doi.org/10.1016/S0360-3199(00)00024-0.

[9] C.J. Yang, R.B. Jackson, China's growing methanol economy and its implications for energy and the environment, Energy Policy. 41 (2012) 878–884. https://doi.org/10.1016/j.enpol.2011.11.037.

[10] I. Janajreh, I. Adeyemi, S.S. Raza, C. Ghenai, A review of recent developments and future prospects in gasification systems and their modeling, Renew. Sustain. Energy Rev. 138 (2021) 110505. https://doi.org/10.1016/j.rser.2020.110505.

[11] P. v. Zedtwitz, A. Steinfeld, The solar thermal gasification of coal - Energy conversion efficiency and CO2 mitigation potential, Energy. 28 (2003) 441–456. https://doi.org/10.1016/S0360-5442(02)00139-1.

[12] D.W. Gregg, R.W. Taylor, J.H. Campbell, J.R. Taylor, A. Cotton, Solar gasification of coal, activated carbon, coke and coal and biomass mixtures, Sol. Energy. 25 (1980) 353–364. https://doi.org/10.1016/0038-092X(80)90347-3.

[13] T. Kodama, N. Gokon, S.I. Enomoto, S. Itoh, T. Hatamachi, Coal coke gasification in a windowed solar chemical reactor for beam-down optics, J. Sol. Energy Eng. Trans. ASME. 132 (2010) 1–6. https://doi.org/10.1115/1.4002081.

[14] A. Z'Graggen, P. Haueter, D. Trommer, M. Romero, J.C. de Jesus, A. Steinfeld, Hydrogen production by steam-gasification of petroleum coke using concentrated solar power-II Reactor design, testing, and modeling, Int. J. Hydrogen Energy. 31 (2006) 797–811. https://doi.org/10.1016/j.ijhydene.2005.06.011.

[15] H. Weldekidan, V. Strezov, G. Town, Review of solar energy for biofuel extraction, Renew. Sustain. Energy Rev. 88 (2018) 184–192. https://doi.org/10.1016/j.rser.2018.02.027.

[16] H. Wu, Q. Liu, Z. Bai, G. Xie, J. Zheng, B. Su, Thermodynamics analysis of a novel steam/air biomass gasification combined cooling, heating and power system with solar energy, Appl. Therm. Eng. 164 (2020) 114494. https://doi.org/10.1016/j.applthermaleng.2019.114494.

[17] N. Gokon, S. Kumaki, Y. Miyaguchi, S. Bellan, T. Kodama, H. Cho, Development of a 5kWth internally circulating fluidized bed reactor containing quartz sand for continuously-fed coal-coke gasification and a beam-down solar concentrating system, Energy. 166 (2019) 1–16. https://doi.org/10.1016/j.energy.2018.10.036.

[18] Q. Bellouard, S. Rodat, S. Abanades, S. Ravel, P.É. Frayssines, Design, simulation and experimental study of a directly-irradiated solar chemical reactor for hydrogen and syngas production from continuous solar-driven wood biomass gasification, Int. J. Hydrogen Energy. 4 (2019) 19193–19205. https://doi.org/10.1016/j.ijhydene.2018.04.147.

[19] F. Müller, H. Patel, D. Blumenthal, P. Poživil, P. Das, C. Wieckert, P. Maiti, S. Maiti, A. Steinfeld, Co-production of syngas and potassium-based fertilizer by solar-driven

thermochemical conversion of crop residues, Fuel Process. Technol. 171 (2018) 89–99. https://doi.org/10.1016/j.fuproc.2017.08.006.
[20] N. Piatkowski, C. Wieckert, A.W. Weimer, A. Steinfeld, Solar-driven gasification of carbonaceous feedstock - A review, Energy Environ. Sci. 4 (2011) 73–82. https://doi.org/10.1039/c0ee00312c.
[21] N. Piatkowski, A. Steinfeld, Solar-driven coal gasification in a thermally irradiated packed-bed reactor, Energy and Fuels. 22 (2008) 2043–2052. https://doi.org/10.1021/ef800027c.
[22] A. Muroyama, T. Shinn, R. Fales, P.G. Loutzenhiser, Modeling of a Dynamically-Controlled Hybrid Solar/Autothermal Steam Gasi fi cation Reactor, (2014).
[23] N. Gokon, R. Ono, T. Hatamachi, L. Liuyun, H.J. Kim, T. Kodama, CO2 gasification of coal cokes using internally circulating fluidized bed reactor by concentrated Xe-light irradiation for solar gasification, Int. J. Hydrogen Energy. 37 (2012) 12128–12137. https://doi.org/10.1016/j.ijhydene.2012.05.133.
[24] T. Kodama, Y. Kondoh, T. Tamagawa, A. Funatoh, K.-I. Shimizu, Y. Kitayama, Fluidized Bed Coal Gasification with CO 2 under Direct Irradiation with Concentrated Visible Light, Energy & Fuels. 16 (2002) 1264–1270. https://doi.org/10.1021/ef020053x.
[25] M. Mehrpooya, M. Dehqani, S.A. Mousavi, S.A. Moosavian, Heat transfer and economic analyses of using various nanofluids in shell and tube heat exchangers for the cogeneration and solar-driven organic Rankine cycle systems, Int. J. Low-Carbon Technol. 17 (2022) 11–22. https://doi.org/10.1093/ijlct/ctab075.
[26] S.A. Mousavi, M. Mehrpooya, M.A.V. Rad, M.H. Jahangir, A new decision-making process by integration of exergy analysis and techno-economic optimization tool for the evaluation of hybrid renewable systems, Sustain. Energy Technol. Assessments. 45 (2021) 101196. https://doi.org/10.1016/j.seta.2021.101196.
[27] S.A. Mousavi, M. Mehrpooya, M. Delpisheh, Development and life cycle assessment of a novel solar-based cogeneration configuration comprised of diffusion-absorption refrigeration and organic Rankine cycle in remote areas, Process Saf. Environ. Prot. 159 (2022) 1019–1038. https://doi.org/10.1016/j.psep.2022.01.067.
[28] X. Cai, S. Shan, Q. Zhang, J. Zhao, Z. Zhou, New WSGG model for gas mixtures of H2O, CO2, and CO in typical coal gasifier conditions, Fuel. 311 (2022) 122541. https://doi.org/10.1016/j.fuel.2021.122541.
[29] E. Terrell, C.S. Theegala, Thermodynamic simulation of syngas production through combined biomass gasification and methane reformation, Sustain. Energy Fuels. 3 (2019) 1562–1572. https://doi.org/10.1039/C8SE00638E.
[30] Y. Bai, P. Lv, F. Li, X. Song, W. Su, G. Yu, Investigation into Ca/Na compounds catalyzed coal pyrolysis and char gasification with steam, Energy Convers. Manag. 184 (2019) 172–179. https://doi.org/10.1016/j.enconman.2019.01.063.
[31] J. Kopyscinski, R. Habibi, C.A. Mims, J.M. Hill, K2CO3-Catalyzed CO2 Gasification of Ash-Free Coal: Kinetic Study, Energy & Fuels. 27 (2013) 4875–4883.
[32] J. Kopyscinski, M. Rahman, R. Gupta, C.A. Mims, J.M. Hill, K2CO3 catalyzed CO2 gasification of ash-free coal. Interactions of the catalyst with carbon in N2 and CO2 atmosphere, Fuel. 117 (2014) 1181–1189. https://doi.org/10.1016/j.fuel.2013.07.030.
[33] S. Islam, J. Kopyscinski, S.C. Liew, J.M. Hill, Impact of K2CO3 catalyst loading on the CO2-gasification of Genesse raw coal and low-ash product, Powder Technol. 290 (2016) 141–147. https://doi.org/10.1016/j.powtec.2015.12.013.
[34] X. Zhou, W. Li, R. Mabon, L.J. Broadbelt, A mechanistic model of fast pyrolysis of hemicellulose, Energy Environ. Sci. 11 (2018) 1240–1260. https://doi.org/10.1039/c7ee03208k.
[35] K.J. Laidler, The development of the arrhenius equation, J. Chem. Educ. 61 (1984) 494–498. https://doi.org/10.1021/ed061p494.
[36] J.C.G. da Silva, J.L.F. Alves, W.V. de A. Galdino, S.L.F. Andersen, R.F. de Sena, Pyrolysis kinetic evaluation by single-step for waste wood from reforestation, Waste Manag. 72 (2018) 265–273. https://doi.org/10.1016/j.wasman.2017.11.034.
[37] S.R. Naqvi, R. Tariq, Z. Hameed, I. Ali, M. Naqvi, W.H. Chen, S. Ceylan, H. Rashid, J. Ahmad, S.A. Taqvi, M. Shahbaz, Pyrolysis of high ash sewage sludge: Kinetics and thermodynamic analysis using Coats-Redfern method, Renew. Energy. 131 (2019) 854–860. https://doi.org/10.1016/j.renene.2018.07.094.
[38] P. Li, Q. Yu, Q. Qin, W. Lei, Kinetics of CO2/coal gasification in molten blast furnace slag,

Ind. Eng. Chem. Res. 51 (2012) 15872–15883. https://doi.org/10.1021/ie301678s.
[39] S. Shan, Z. Zhou, Z. Wang, K. Cen, A novel flame energy grading conversion system: Preliminary experiment and thermodynamic parametric analysis, Int. J. Energy Res. 44 (2020) 2084–2099. https://doi.org/10.1002/er.5066.
[40] A.S. Joshi, I. Dincer, B. V. Reddy, Performance analysis of photovoltaic systems: A review, Renew. Sustain. Energy Rev. 13 (2009) 1884–1897. https://doi.org/10.1016/j.rser.2009.01.009.
[41] C. Michalakakis, A.G. Hernandez, J. Fouillou, J.M. Cullen, R.C. Lupton, Calculating the chemical exergy of materials, J. Ind. Ecol. (2021) 274–287. https://doi.org/10.1111/jiec.13120.
[42] M. Gräbner, B. Meyer, Performance and exergy analysis of the current developments in coal gasification technology, Fuel. 116 (2014) 910–920. https://doi.org/10.1016/j.fuel.2013.02.045.
[43] J.M. Sanchez-Hervas, G.M. Moya, I. Ortiz-González, Current status of coal gasification, New Trends Coal Convers. Combust. Gasification, Emiss. Coking. (2018) 175–202. https://doi.org/10.1016/B978-0-08-102201-6.00007-8.
[44] Z. Zhou, Q. Zhang, L. Chen, Experimental Analysis of Intrinsic Kinetics and Rate Profiles for Coal Char Conversion under Different Atmospheres, Combust. Sci. Technol. 00 (2021) 1–18. https://doi.org/10.1080/00102202.2021.1973448.
[45] A. Sharma, T. Takanohashi, I. Saito, Effect of catalyst addition on gasification reactivity of HyperCoal and coal with steam at 775-700 °C, Fuel. 87 (2008) 2686–2690. https://doi.org/10.1016/j.fuel.2008.03.010.
[46] L. Xu, J. Yuan, Thermodynamic properties calculation of the flue gas based on its composition estimation for coal-fired power plants, Appl. Therm. Eng. 90 (2015) 366–375. https://doi.org/10.1016/j.applthermaleng.2015.07.018.
[47] N. Fang, L. Zeng, B. Zhang, Z. Li, H. Wang, X. Liu, Numerical simulation of flow and gasification characteristics with different swirl vane angles in a 2000 t/d GSP gasifier, Appl. Therm. Eng. 153 (2019) 791–799. https://doi.org/10.1016/j.applthermaleng.2019.03.006.
[48] C.M. Administration, https://en.wikipedia.org/wiki/Hangzhou, (n.d.).
[49] S. Sukumaran, K. Sudhakar, Performance analysis of solar powered airport based on energy and exergy analysis, Energy. 149 (2018) 1000–1009. https://doi.org/10.1016/j.energy.2018.02.095.
[50] A. Kasaeian, A. Kouravand, M.A. Vaziri Rad, S. Maniee, F. Pourfayaz, Cavity receivers in solar dish collectors: A geometric overview, Renew. Energy. 169 (2021) 53–79. https://doi.org/10.1016/j.renene.2020.12.106.
[51] T. Kodama, Y. Kondoh, T. Tamagawa, A. Funatoh, K.I. Shimizu, Y. Kitayama, Fluidized bed coal gasification with CO2 under direct irradiation with concentrated visible light, Energy and Fuels. 16 (2002) 1264–1270. https://doi.org/10.1021/ef020053x.
[52] X. Li, J. Chen, Q. Hu, P. Chu, Y. Dai, C.-H. Wang, Solar-driven gasification in an indirectly-irradiated thermochemical reactor with a clapboard-type internally-circulating fluidized bed, Energy Convers. Manag. 248 (2021) 114795. https://doi.org/10.1016/j.enconman.2021.114795.
[53] W.B. Stine, R.B. Diver, A compendium of solar dish/Stirling technology, SAND93-7026 UC-236, (1994). http://www.osti.gov/energycitations/servlets/purl/10130410-xiVU1V/native/%5Cn10.2172/10130410.
[54] S.Y. Wu, L. Xiao, Y. Cao, Y.R. Li, Convection heat loss from cavity receiver in parabolic dish solar thermal power system: A review, Sol. Energy. 84 (2010) 1342–1355. https://doi.org/10.1016/j.solener.2010.04.008.
[55] R. Lanzafame, M. Messina, A new method for the calculation of gases enthalpy, in: 35th Intersoc. Energy Convers. Eng. Conf. Exhib., 2000: pp. 318–328.
[56] M. Boxwell, Solar electricity handbook: A simple, practical guide to solar energy-designing and installing photovoltaic solar electric systems, Greenstream publishing, 2010.

Declaration of interests

The authors declare that they have no known competing financial interests or personal relationships that could have appeared to influence the work reported in this paper.